


FULL PAPER

Open Access



# Seismic velocity structure along the Sea of Japan with large events derived from seismic tomography for whole Japanese Islands including reflection survey data and NIED MOWLAS Hi-net and S-net data

Makoto Matsubara<sup>1\*</sup> , Tatsuya Ishiyama<sup>2</sup>, Tetsuo No<sup>3</sup>, Kenji Uehira<sup>1</sup>, Masashi Mochizuki<sup>1</sup>, Toshihiko Kanazawa<sup>4</sup>, Narumi Takahashi<sup>1</sup> and Shin'ichiro Kamiya<sup>1</sup>

## Abstract

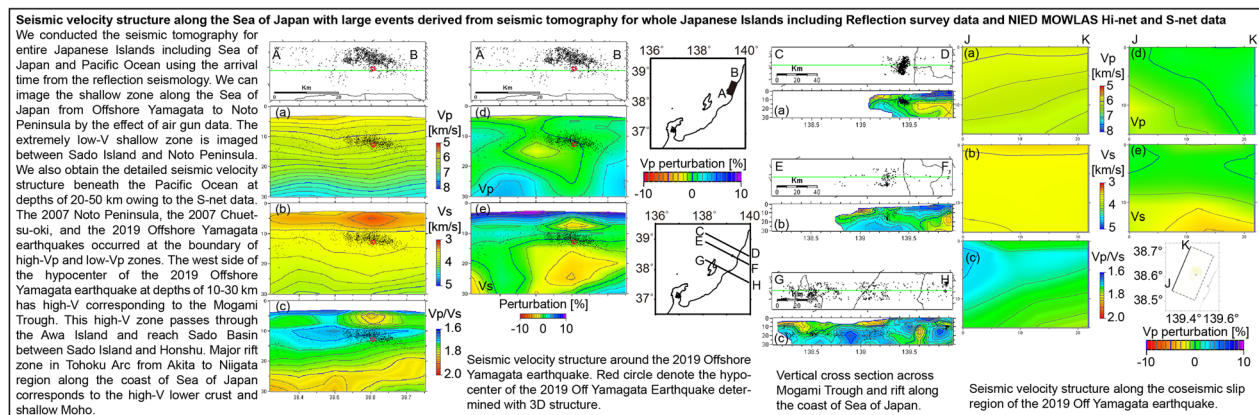
We conducted seismic tomography for entire Japanese Islands including the Sea of Japan and the Pacific Ocean using arrival times from reflection survey as well as the routine seismic network. We successfully imaged the shallow zone along the Sea of Japan from offshore Yamagata to the Noto Peninsula by using air gun data. An extremely low- $V$  shallow zone is imaged between Sado Island and Noto Peninsula. We also obtained detailed seismic velocity structure beneath the Pacific Ocean at depths of 20–50 km using S-net data. The 2007 Noto Peninsula, the 2007 offshore Chuetsu, and the 2019 offshore Yamagata earthquakes occurred at the boundary between high- $V_p$  and low- $V_p$  zones. The west side of the hypocenter of the 2019 offshore Yamagata earthquake at depths of 10–30 km has high- $V$  corresponding to the Mogami Trough. This high- $V$  zone passes through Awa Island and reaches Sado Basin between Sado Island and Honshu. A major rift zone in the Tohoku Arc extending from the Akita region to the Niigata region along the coast of Sea of Japan corresponds to high- $V$  lower crust and a shallow Moho.

**Keywords:** Seismic tomography, Sea of Japan, Failed rift, NIED S-net, NIED Hi-net

\*Correspondence: [mkmatsu@bosai.go.jp](mailto:mkmatsu@bosai.go.jp)

<sup>1</sup> National Research Institute for Earth Science and Disaster Resilience, 3-1 Tennodai, Tsukuba, Ibaraki 305-0006, Japan  
Full list of author information is available at the end of the article

## Graphical Abstract



## Introduction

The seismic velocity structure beneath the Japanese Islands is extremely complex because the Japanese Islands consist of the Eurasian (EUR), the North American (NA), and the Philippine Sea (PHS) plates where the PHS and the Pacific (PAC) plates subduct beneath the EUR and the NA plates (Fig. 1, tectonic setting). The National Research Institute for Earth Science and Disaster Resilience (NIED) deployed a nation-wide high-sensitivity seismograph network (Hi-net) according to the Special Measure Law on Earthquake Disaster Prevention after the Kobe earthquake in January 1995 since NIED had already accumulated experience from the Tokyo metropolitan deep borehole array and had operated the Kanto-Tokai seismic network since 1979 (National Research Institute for Earth Science and Disaster Resilience 2019a). NIED started operation of Hi-net in 2000 (Okada et al. 2004; Obara et al. 2005). The Japan Meteorological Agency (JMA), the National Universities, and other institutes operate other seismic networks for the detection of microseismicity. An ocean bottom seismic network is operated in Sagami Bay by NIED, off Tokai and Boso by JMA, offshore Sanriku by the Earthquake Research Institute, the University of Tokyo, offshore Kushiro and Muroto by the Japan Agency for Marine-Earth Science and Technology (JAMSTEC). JAMSTEC constructed the Dense Oceanfloor Network System for Earthquakes and Tsunamis (DONET) (National Research Institute for Earth Science and Disaster Resilience 2019b) offshore Kii peninsula and Point Muroto near the Nankai Trough, and they started operation of DONET offshore Kii (in 2014) and Muroto (in 2016) Peninsulas. NIED deployed the Seafloor Observation Network for Earthquakes and Tsunamis along the Japan Trench (S-net)

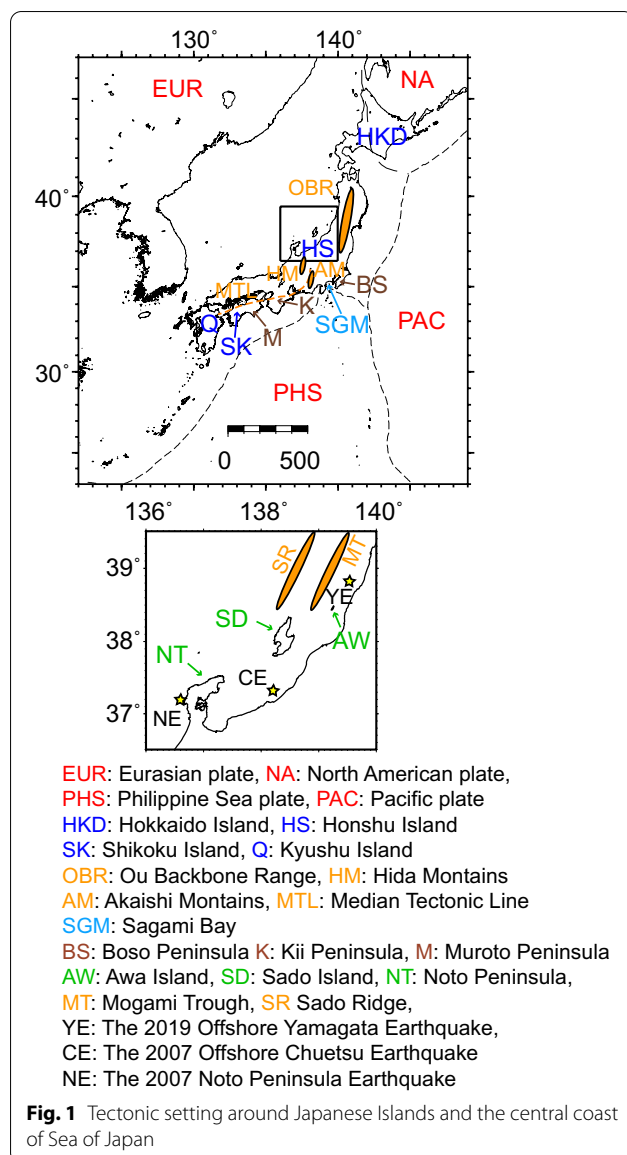
(National Research Institute for Earth Science and Disaster Resilience 2019d) after the 2011 offshore Tohoku Earthquake (the Tohoku-oki event) and began operating in 2016 (Kanazawa 2013; Uehira et al. 2016). DONET was transferred to NIED from April 2016. NIED started operation of Monitoring of Waves on Land and Seafloor (MOWLAS) consisting of Hi-net, the full range seismograph network (F-net), S-net, DONET, Strong-motion Seismograph Networks (K-NET and KiK-net), and Volcano Observation Network (V-net) (National Research Institute for Earth Science and Disaster Resilience 2019c). These seismic networks contributed to the analysis of three-dimensional (3D) seismic velocity structure (e.g., Matsubara et al. 2005, 2008, 2017b, 2019; Matsubara and Obara 2011). Matsubara et al. (2017b, 2019) combined the arrival time data of the NIED Hi-net and centroid moment tensor data of the NIED F-net data and those using tiltmeters that accompany NIED Hi-net stations (Asano et al. 2011). Because the about 2-year period of S-net data is too short to analyze seismic tomogram; however, we only used the arrival time data at the permanent land stations such as the NIED Hi-net, NIED S-net, JMA, national universities, and the other organizations since the NIED S-net data have been collected for 5 years.

## Data and methods

### Data for seismic tomography

In this study, the target region is 20–48° N and 120–148° E. It covers the entire Japanese Islands from Hokkaido (Kuril Islands) to Okinawa (Ryukyu Islands) and the Pacific Ocean where the seismic stations of onshore Hi-net and offshore the S-net and the DONET are deployed. JAMSTEC conducted the reflection survey in the Sea of





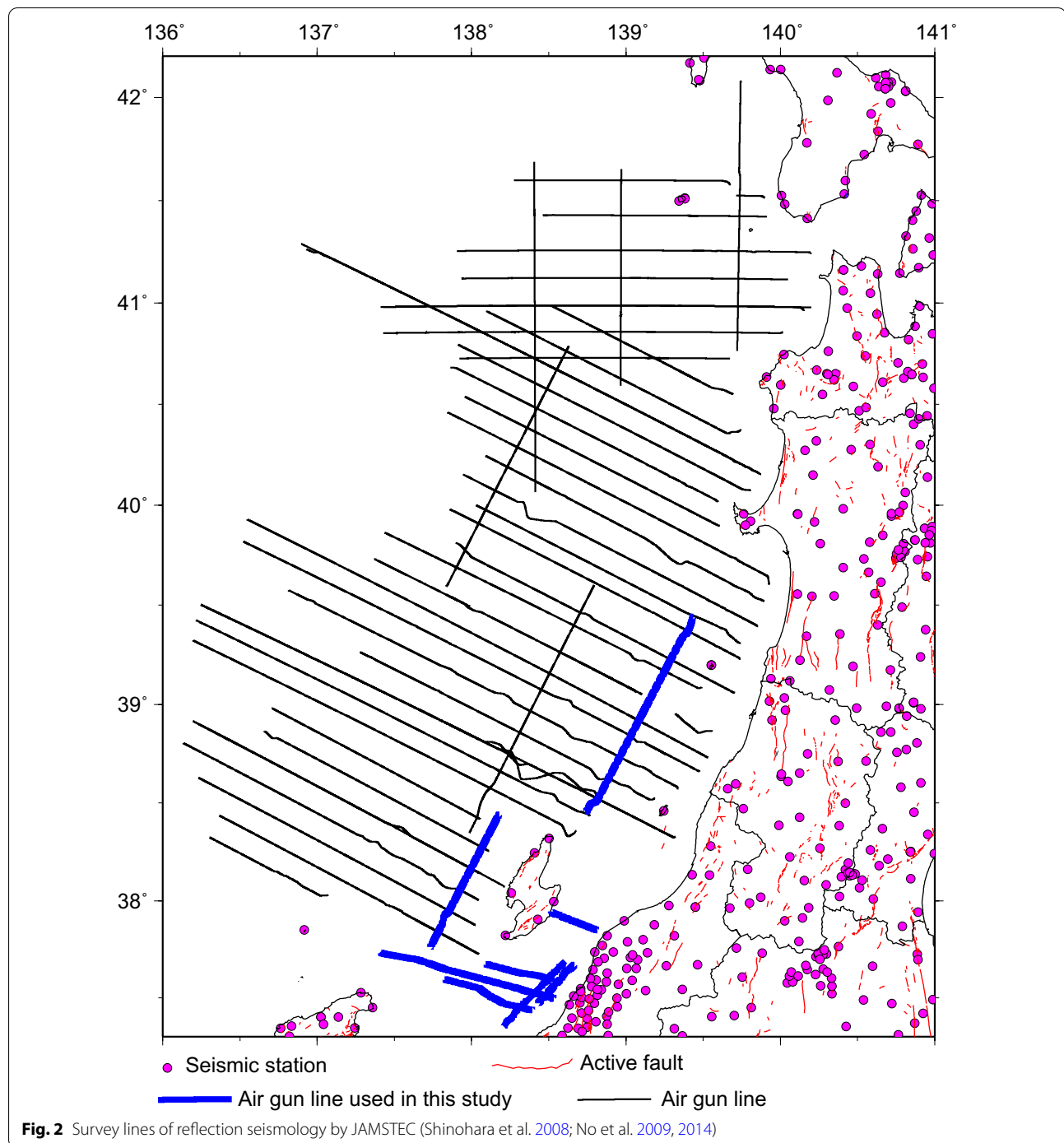
Japan from 2007 to 2011 (Fig. 2) under “Multidisciplinary research project for construction of fault model in the high strain rate zone” and from 2014 to 2020 under “Research project for earthquake and tsunami in the Sea of Japan” by Ministry of Education, Culture, Sports, Science and Technology (MEXT) Japan (Shinohara et al. 2008; No et al. 2009, 2014). In this study, we used the traverse lines near Sado Island and offshore Yamagata prefecture since the traverse lines are surrounded with inland stations and near the source regions of the 2007 offshore Chuetsu Earthquake and the 2019 offshore Yamagata earthquake. JAMSTEC conducted the reflection survey using the air gun shots with an interval of 50 m or 200 m (No et al. 2014). The original intervals of air gun shots are

50 m or 200 m. We superimposed the signals from five or nine consecutive shots to create an interval of 1 km for shot points (Fig. 3). The superposition of nine signals increases the S/N ratio by a factor of three. The reflected seismic signals reach the stations around 150–200 km (Fig. 4). For earthquake data, we selected the hypocenter with the maximum number of phase picks from each box with the size of a horizontal 0.01 degree (approximately 1 km) and 1 km in vertical direction at depths of 0–10 km to match the interval of air guns. At depths greater than 10 km, we similarly selected the earthquake hypocenter from a box with the size of a horizontal 0.1 degree and 2.5 km in vertical direction at depths deeper than 10 km. The number of hypocenters beneath the Pacific Ocean is smaller than the number beneath Japanese Islands since the S-net observation began from 2017. Beneath the Pacific Ocean, we chose the earthquake hypocenter with the maximum number of phase picks from a box with the size of a horizontal 0.01° (approximately 1 km) and 1 km in vertical direction at all depths beneath the Pacific Ocean. We used 14,850,442 P- and 12,278,029 S-wave arrival time data from 294,865 natural sources and 11,089 P-wave arrival time data from 482 air gun shots to constrain the seismic tomography (Fig. 5).

### Seismic tomography

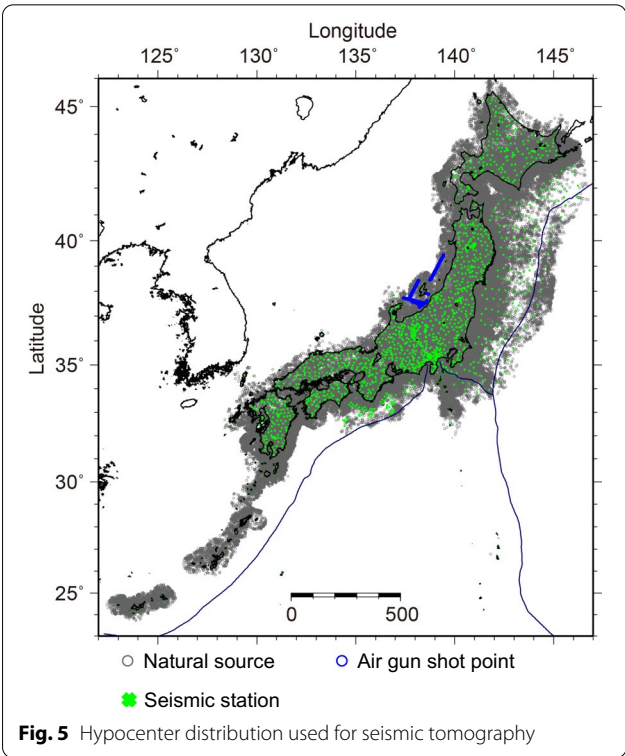
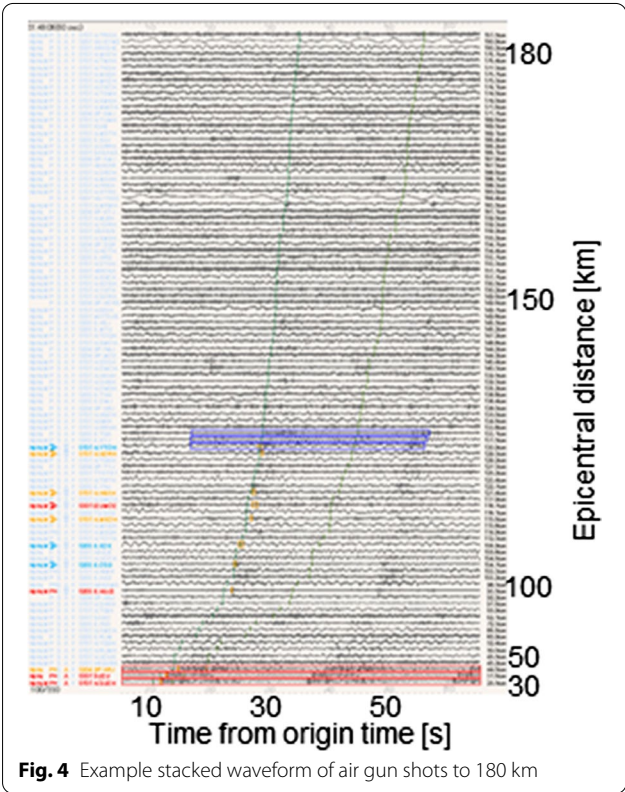
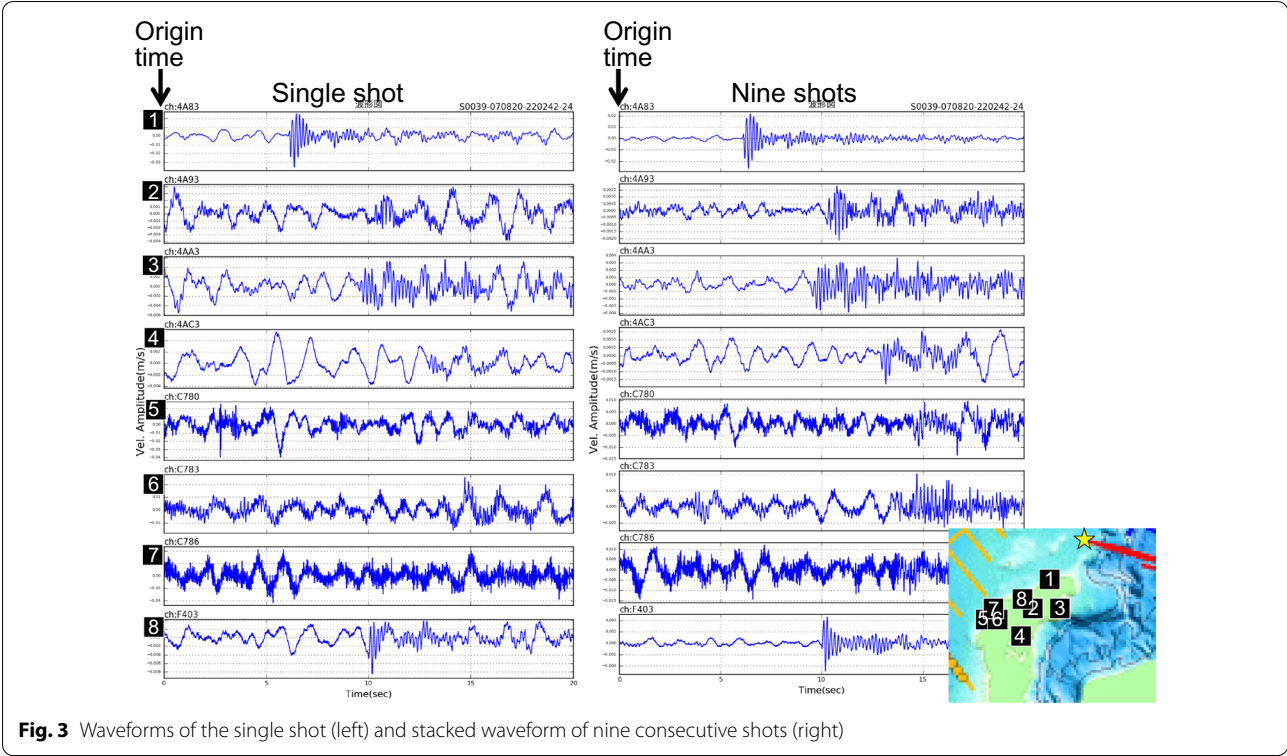
We applied these data to the grid-type tomographic method (Zhao et al. 1992) with spatial velocity correlation and station corrections added to the original code (Matsubara et al. 2004, 2005). We calculated station corrections for P- or S-wave for each seismic station to account for the average residuals for P- or S-wave from all earthquakes. The spacing of grid nodes equals to the resolution size in the original method (Zhao et al. 1992), however, denser grid nodes with the spacing as half of the resolution size were placed (Matsubara et al. 2004, 2005). More grid nodes increase both the ability to match the smallest resolvable size of heterogeneity and the instability of solution. A spatial velocity correlation is introduced to stabilize the solution. We used the LSQR algorithm (Paige and Saunders 1982) extended to an arbitrary damping matrix by Nolet (1987) with a combination of diagonal and smoothing matrices for the stable solution during the inversion, since we placed approximately eight times as many grid nodes compared to the resolution size for the inversion. The pseudo-bending method for ray tracing (Koketsu and Sekine 1998) is used within the 3D structure among the grid nodes.

We used travel-time residuals of less than 0.5 s for P-wave and 0.6 s for S-wave for the inversion of seismic velocity structure. We simultaneously inverted for the 3D seismic structure and the relocated the hypocenters of natural sources. We conducted the inversion of



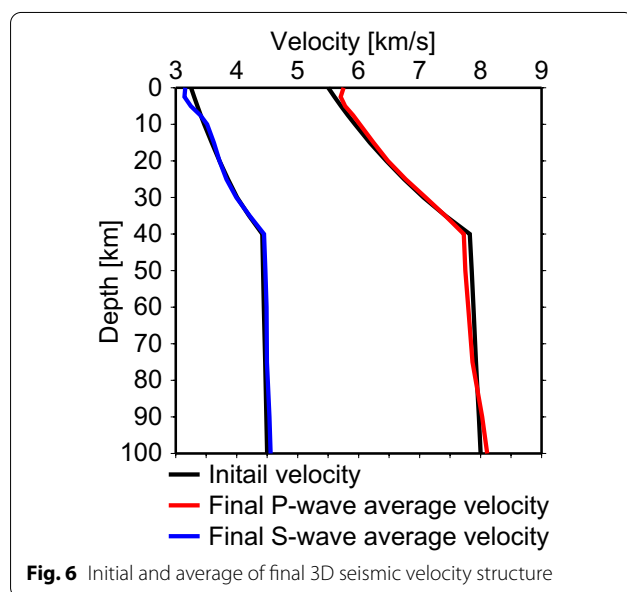
the seismic structure and relocation of natural sources 20 times. We finally used 12,597,329 P- and 7,950,656 S-wave arrival time data for inversion. The inversion reduces root-mean-square of the P-wave travel time residual from 0.471 to 0.165 s and that of the S-wave data from 0.761 to 0.206 s after 20 iterations.

We set up the 3D grid nodes to construct the velocity (slowness) structure with a grid spacing of  $0.1^\circ$  (approximately 10 km) in the horizontal direction. The grid interval in the vertical direction is described in Table. 1. The resolution for the horizontal direction is  $0.2^\circ$  (approximately 20 km), twice of grid interval ( $0.1^\circ$ , 10 km), and



**Table 1** Grid interval and resolution size

Depth	Grid interval		Resolution/ checkerboard pattern	
	Horizontal	Vertical	Horizontal	Vertical
0–10	0.1°	2.5 km	0.2°	5 km
10–40		5 km		10 km
40–60		10 km		20 km
60–180		15 km		30 km
180–300		20 km		40 km
300–		25 km		50 km

**Fig. 6** Initial and average of final 3D seismic velocity structure

that for the vertical direction is also twice the grid interval.

We checked the resolution with the checkerboard resolution test and the restored resolution test. We assumed the  $\pm 5\%$  checkerboard pattern for  $0.2^\circ$  in horizontal and 5–50 km in vertical direction same as the resolution size (Table 1) for the checkerboard resolution test. We calculated the theoretical travel times using the checkerboard pattern and inverted from the initial model for the checkerboard resolution test. We also assumed the final model and calculated the travel times and inverted from the initial model for the restored resolution test. We used only ray paths with residuals less than 0.5 s for P-wave and 0.6 s for S-wave for the final 3D seismic structure used in the inversion in these two resolution tests. We fixed the hypocenters relocated with the final 3D Vp and Vs structures during these tests.

### Initial velocity structure

We adopted the one-dimensional (1D) velocity structures for P- and S-waves used in the NIED Hi-net routine processing as the initial seismic velocity models (Fig. 6; Ukawa et al. 1984). Previous studies assumed the velocity discontinuities as the Moho or the upper boundary of the Pacific Plate (e.g., Zhao et al. 1992, 2011, 2015); however, we can find zones with high velocity gradients without the assumption of velocity discontinuities since many earthquakes occur and many ray paths cross in this region.

## Results

### Results of checkerboard resolution test

Figures 7 and 8 show the results of the checkerboard test for P- and S-waves, respectively. Resolution beneath the four main islands is good at depths of 10–60 km based on the checkerboard resolution test (Figs. 7a–g and 8a–g). The resolution beneath the Pacific Ocean improves at depths greater than 10 km (Figs. 7c–g and 8c–g). We focus on the area of northern central Honshu from Yamagata prefecture to Noto Peninsula with the additional data of reflection survey. Figure 9 shows the checkerboard resolution test results using only natural sources compared to the results including seismic reflection data. We can obtain much better resolution at depths of 0, 5 and 10 km beneath this region (Fig. 9) with the seismic reflection data (with an interval of  $\sim 1$  km) compared to that obtained with only natural sources.

### Map views at depths of 0–60 km for the entire Japanese Islands

Figures 10, 11, 12, 13, 14 show the map views of Vp perturbation, Vs perturbation, and Vp/Vs, restored resolution test for Vp, and that for Vs at depths of 0–400 km, respectively. We calculated the average 1D model from the final 3D velocity structure (Fig. 6). We also show the perturbation of the final 3D velocities from these average velocities (Figs. 10, 11).

At a depth of 5 km, low-Vp zones are located along the Pacific Ocean from Hokkaido to northeastern Kanto region and beneath the southern Kanto region, southern Kii peninsula to southern Shikoku Island. Low-Vp zones are located between the Sado Island and Honshu Island. At a depth of 10 km, low-V zones are located beneath the Kanto region and region between Sado Island and Noto Peninsula, and the southern side of the Median Tectonic Line (MTL). At a depth of 20 km, P-wave and S-wave seismic velocity structures beneath the Pacific Ocean are resolved especially off the eastern Japan. High-V zone is located along the coast of the Pacific Ocean beneath the eastern Japan and low-V zone are located on the east side of the previous high-V zone beneath the Pacific Ocean.



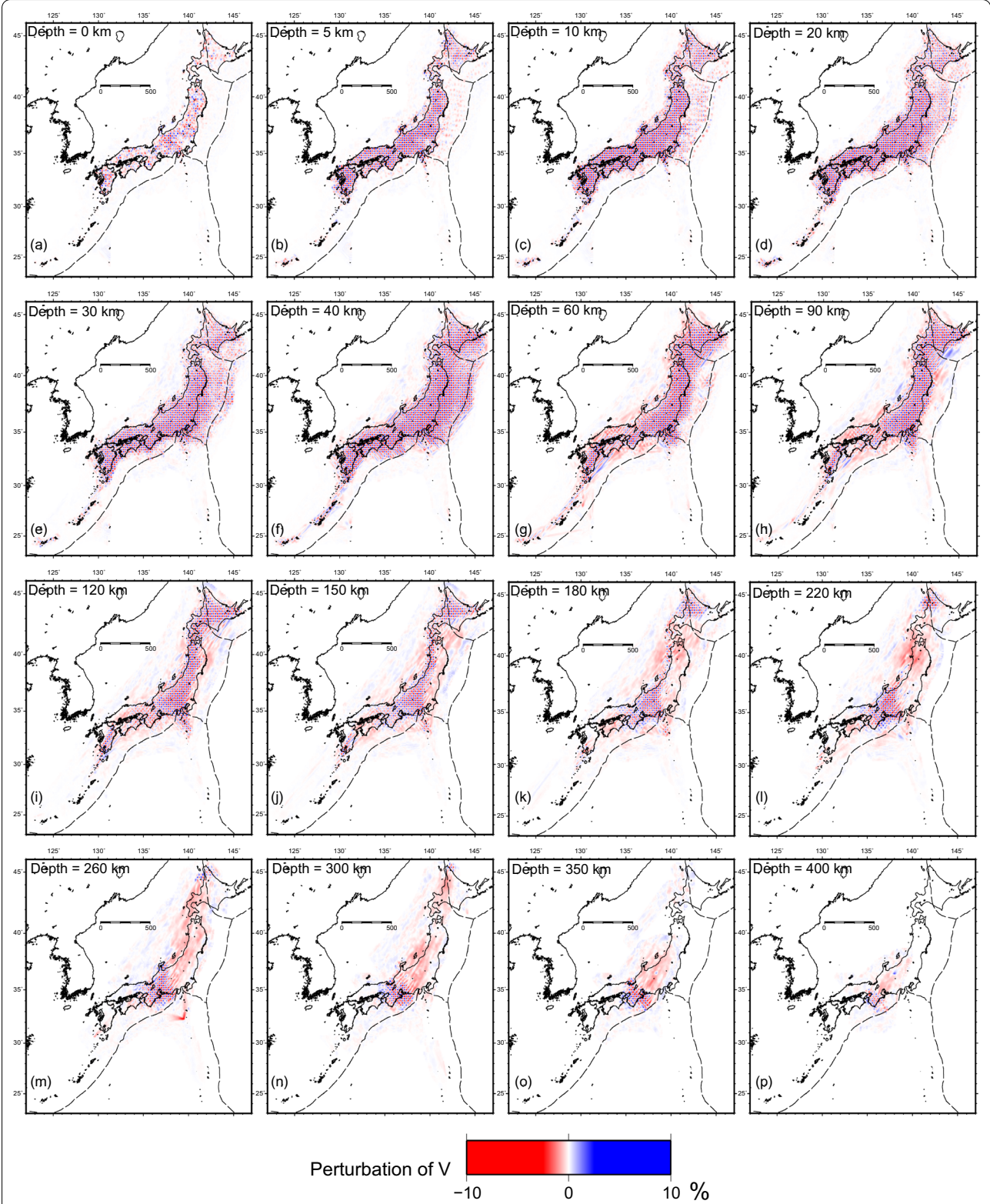


**Fig. 7** Result of checkerboard resolution test for P-wave



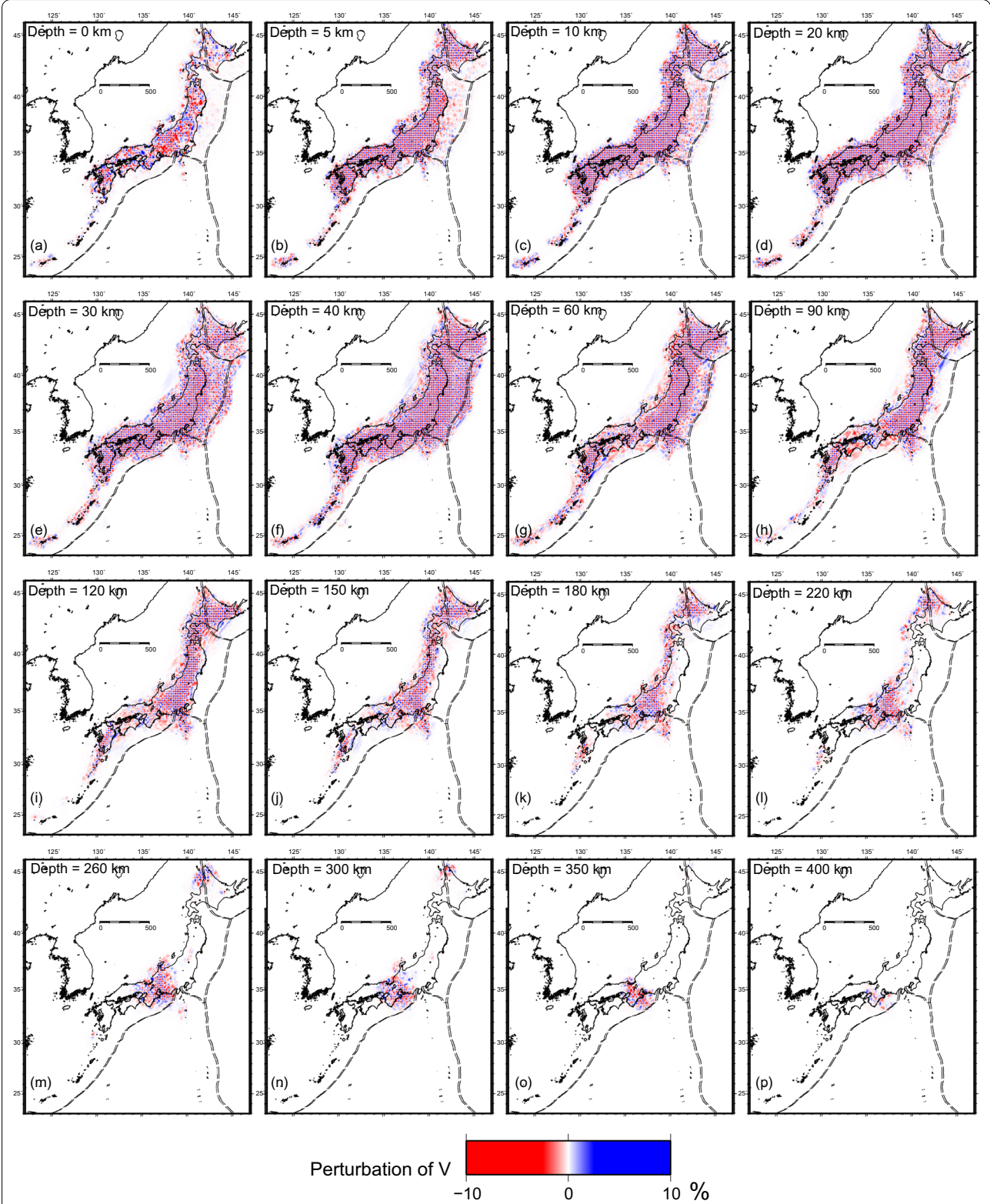


**Fig. 8** Result of checkerboard resolution test for S-wave

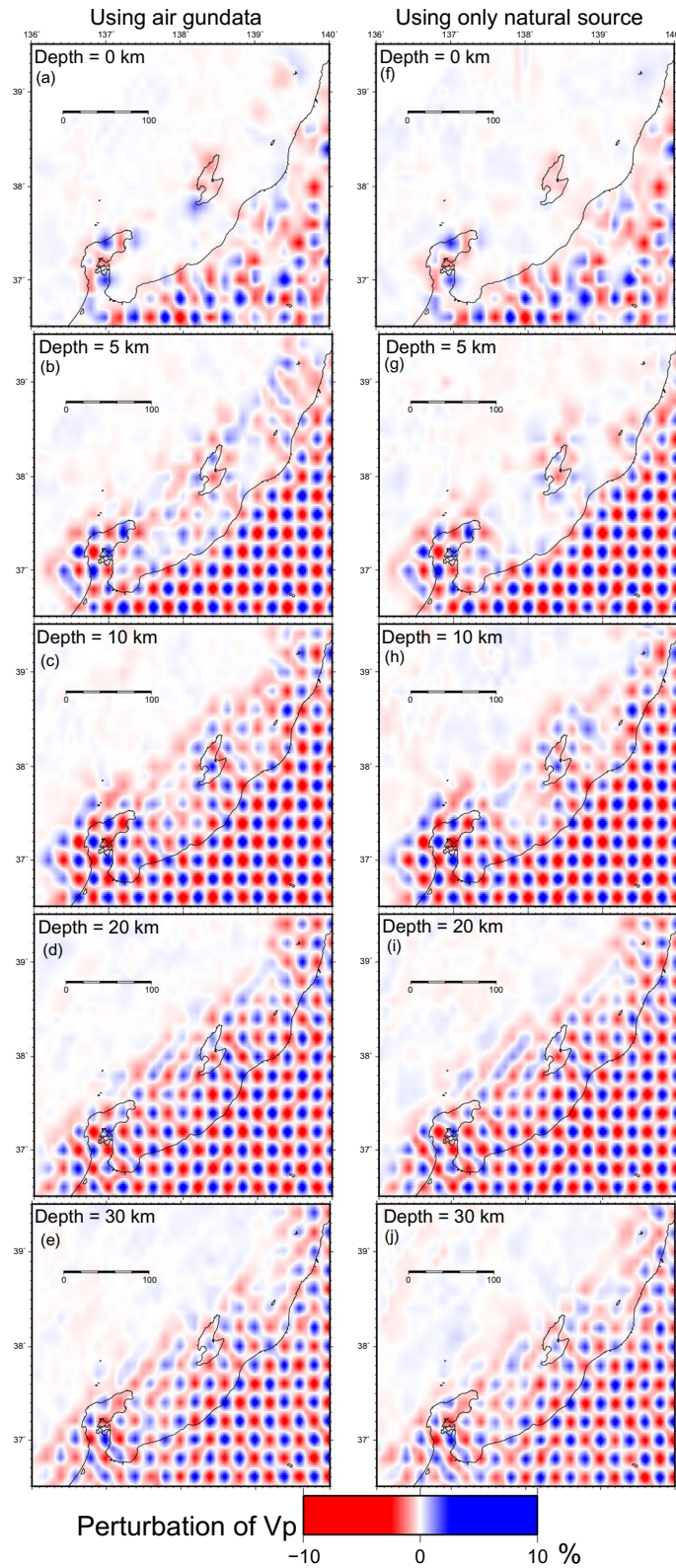


**Fig. 9** Result of checkerboard resolution test with/without reflection seismology at the central coast of Sea of Japan

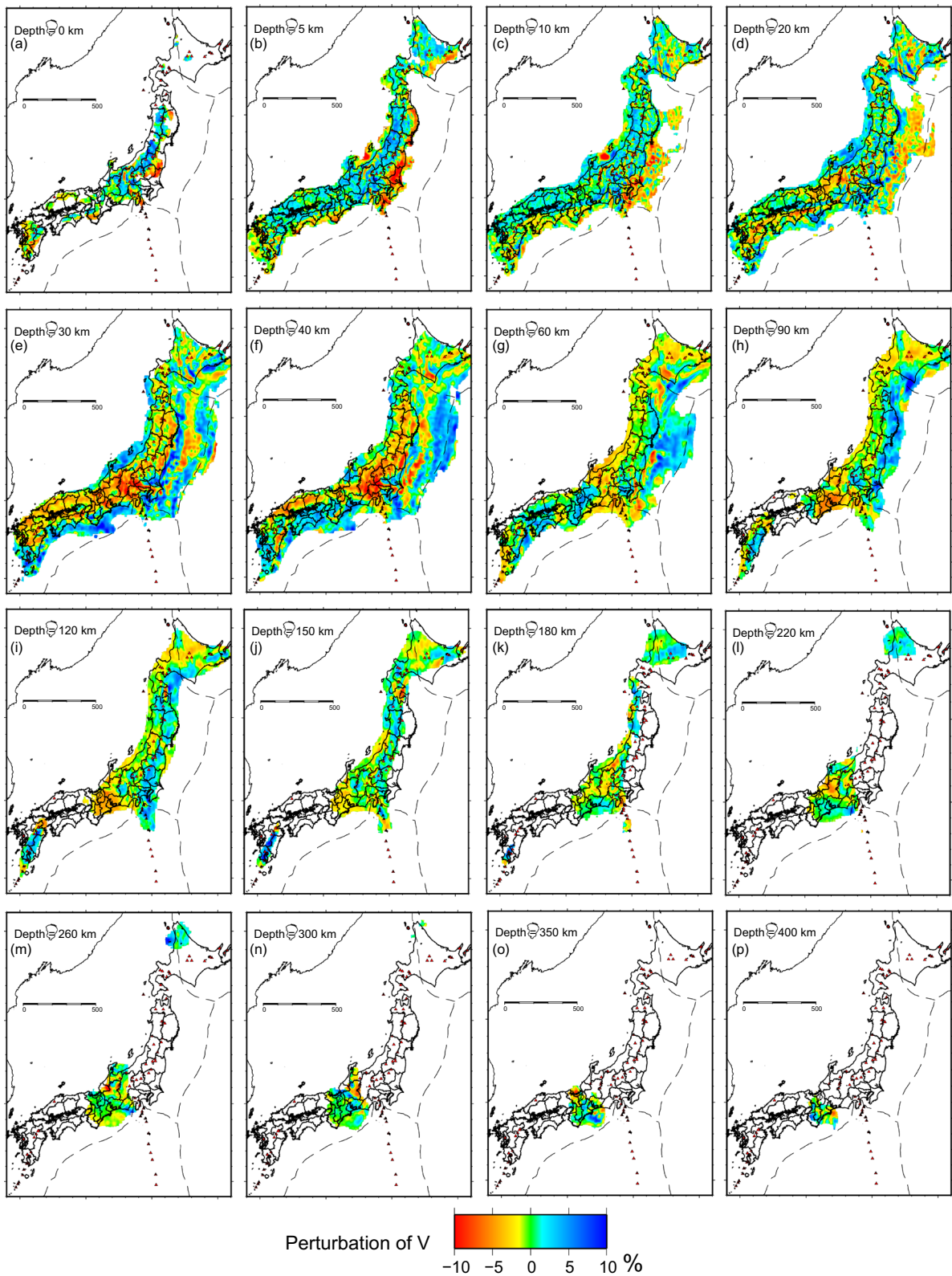


**Fig. 10** Map views of  $V_p$  perturbation beneath Japanese Islands



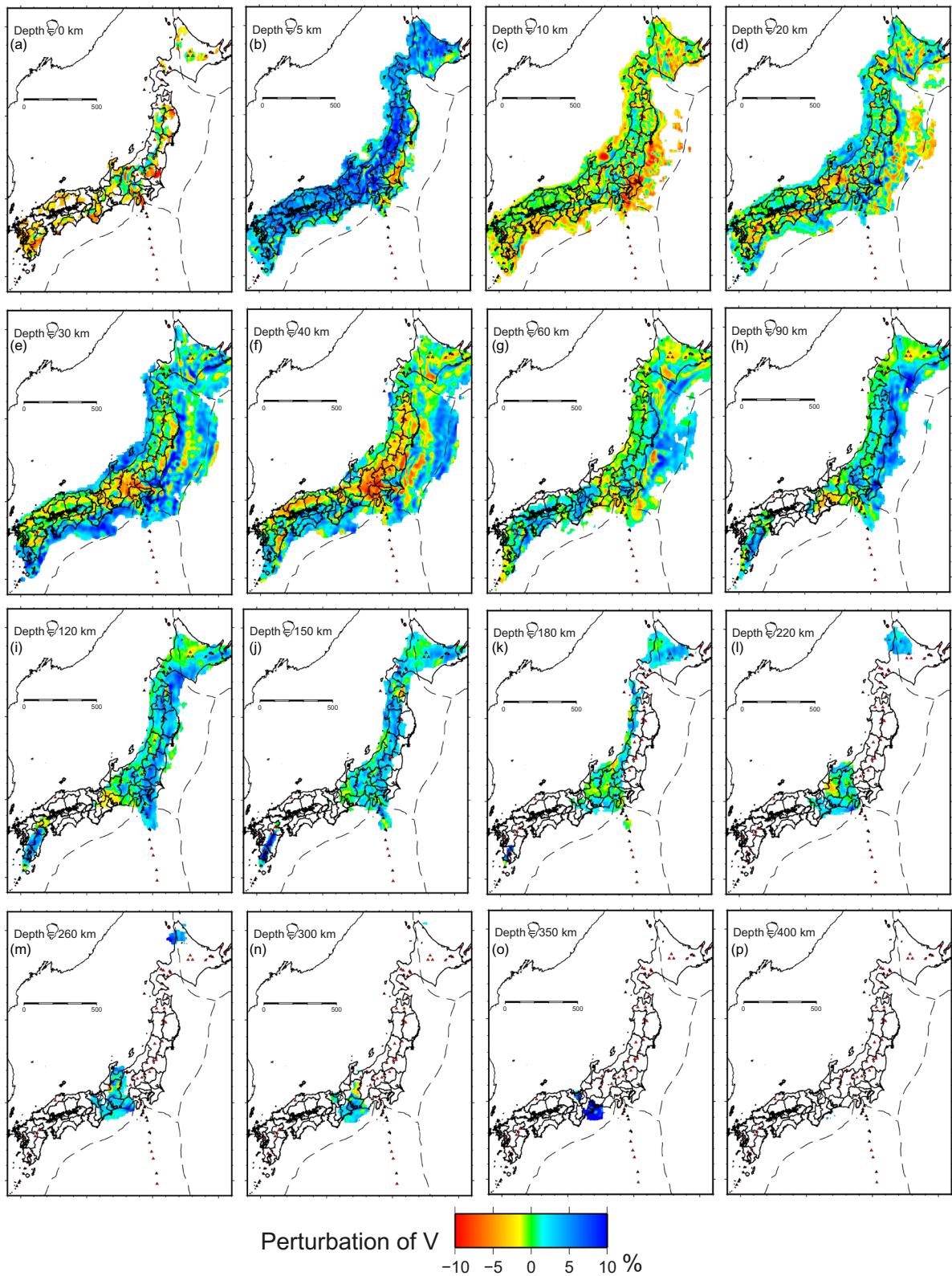


**Fig. 11** Map views of Vs perturbation beneath Japanese Islands

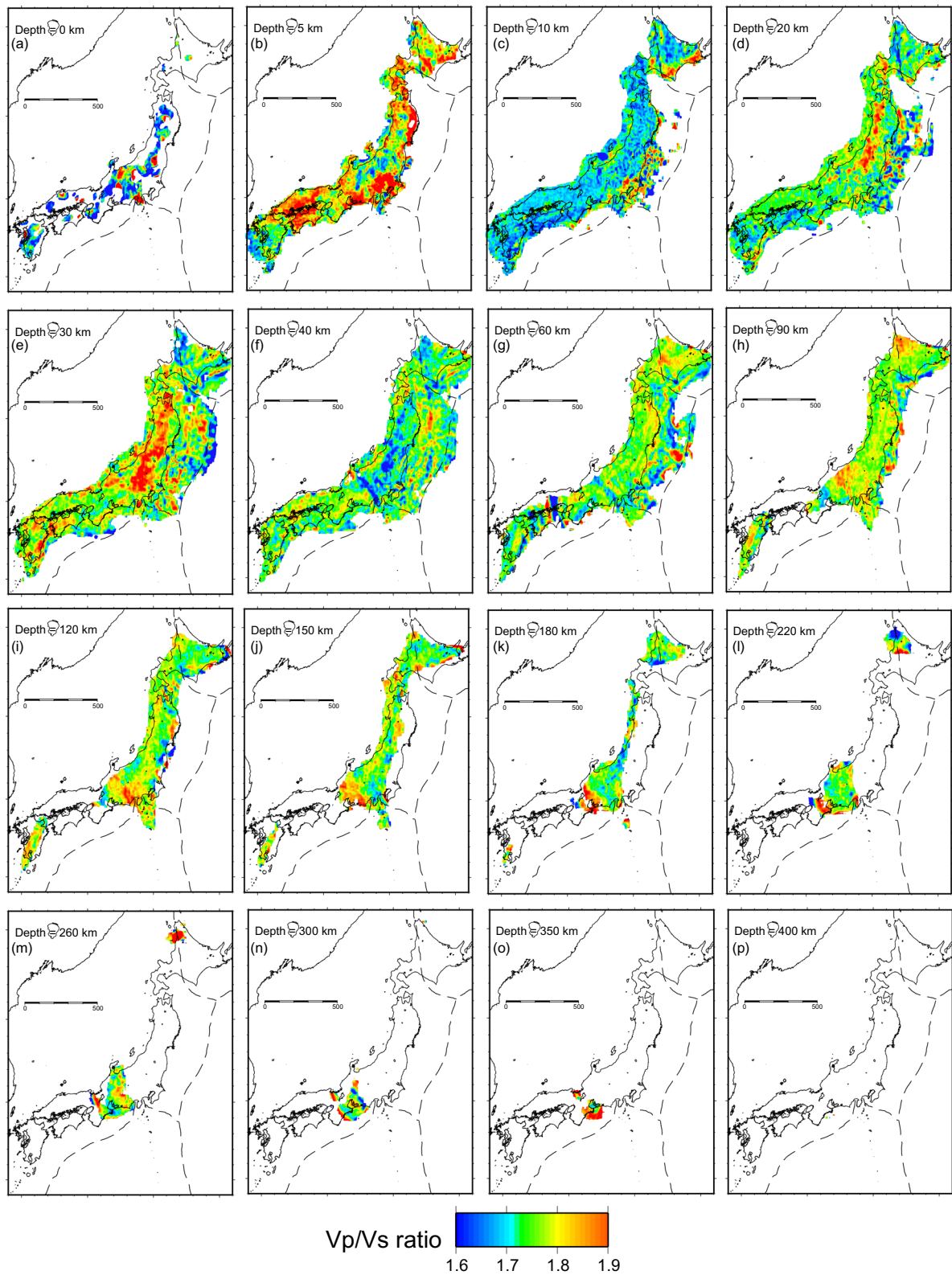


**Fig. 12** Map views of  $V_p/V_s$  beneath Japanese Islands



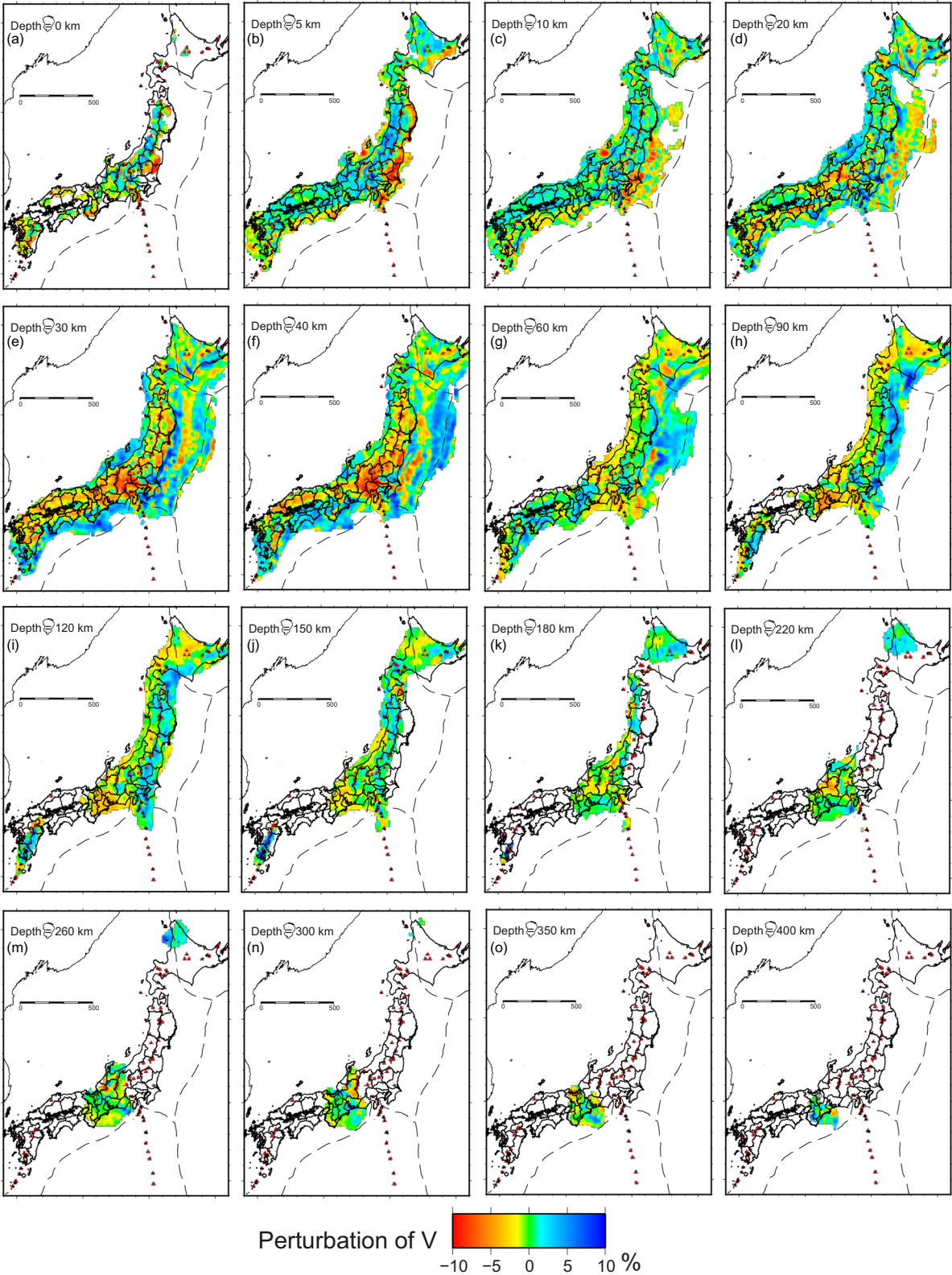


**Fig. 13** Results of restored resolution test for Vp

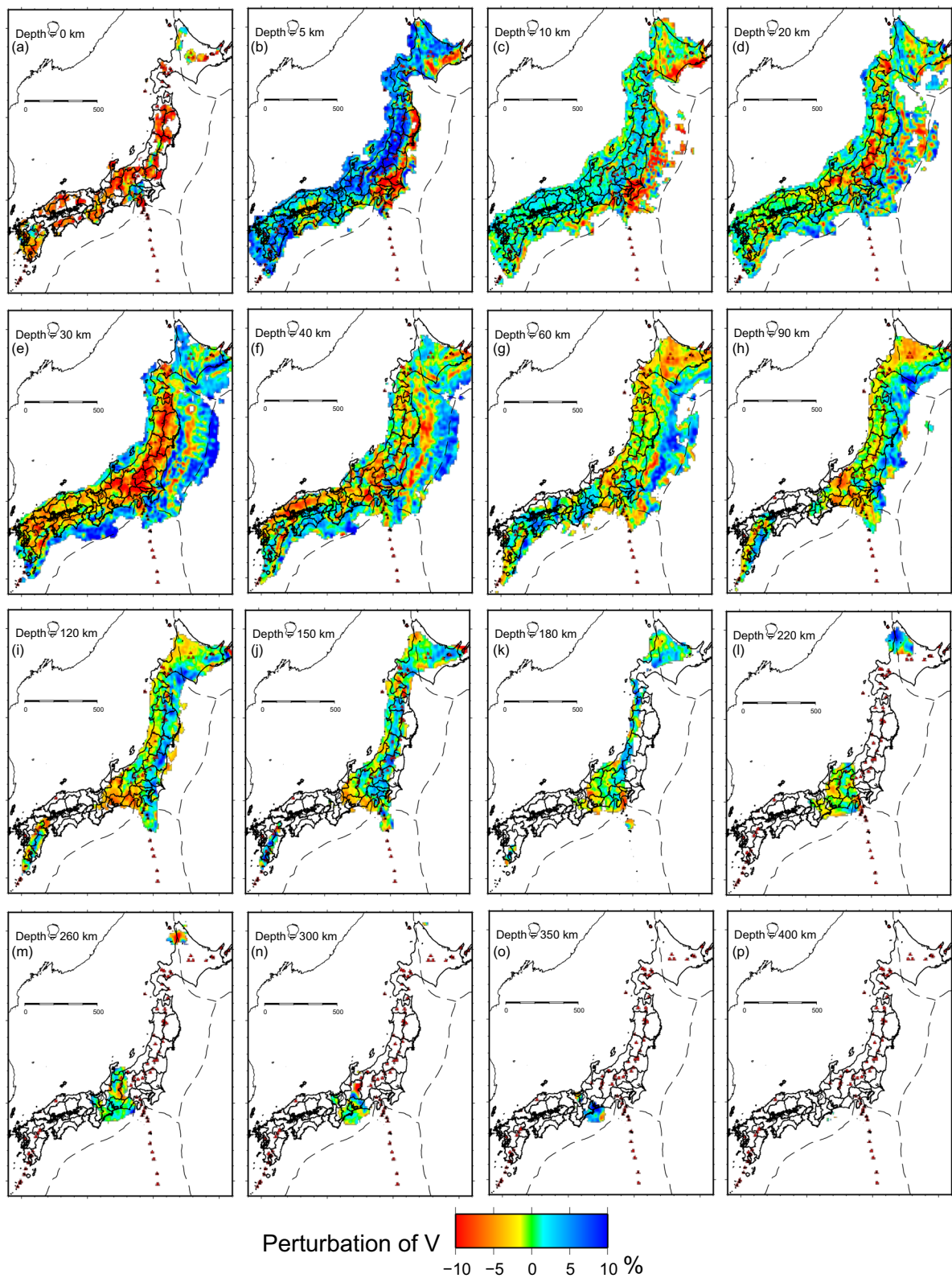


**Fig. 14** Results of restored resolution test for Vs

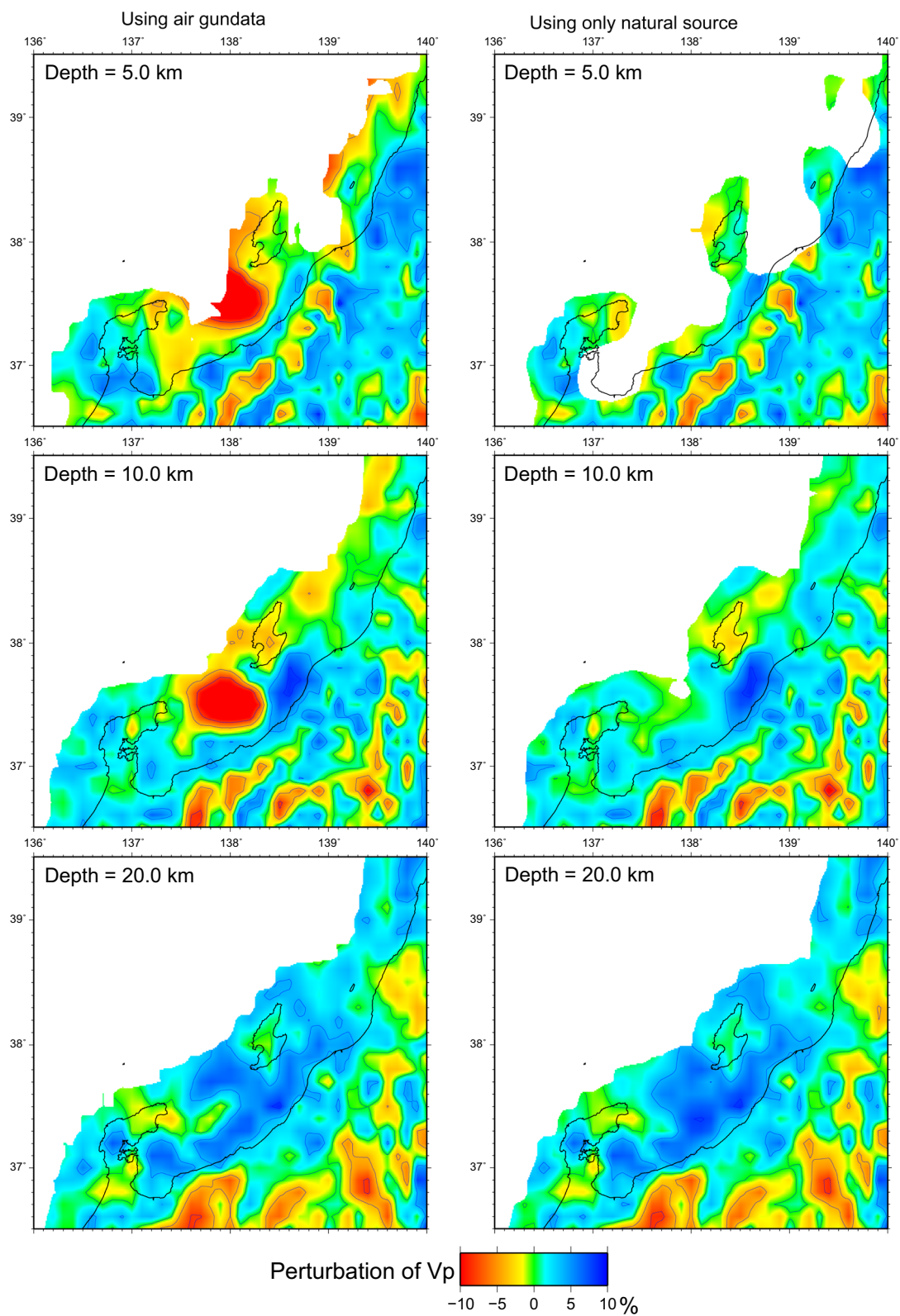


**Fig. 15** Map views of  $V_p$  beneath the central coast of the Sea of Japan from Yamagata to Noto Peninsula



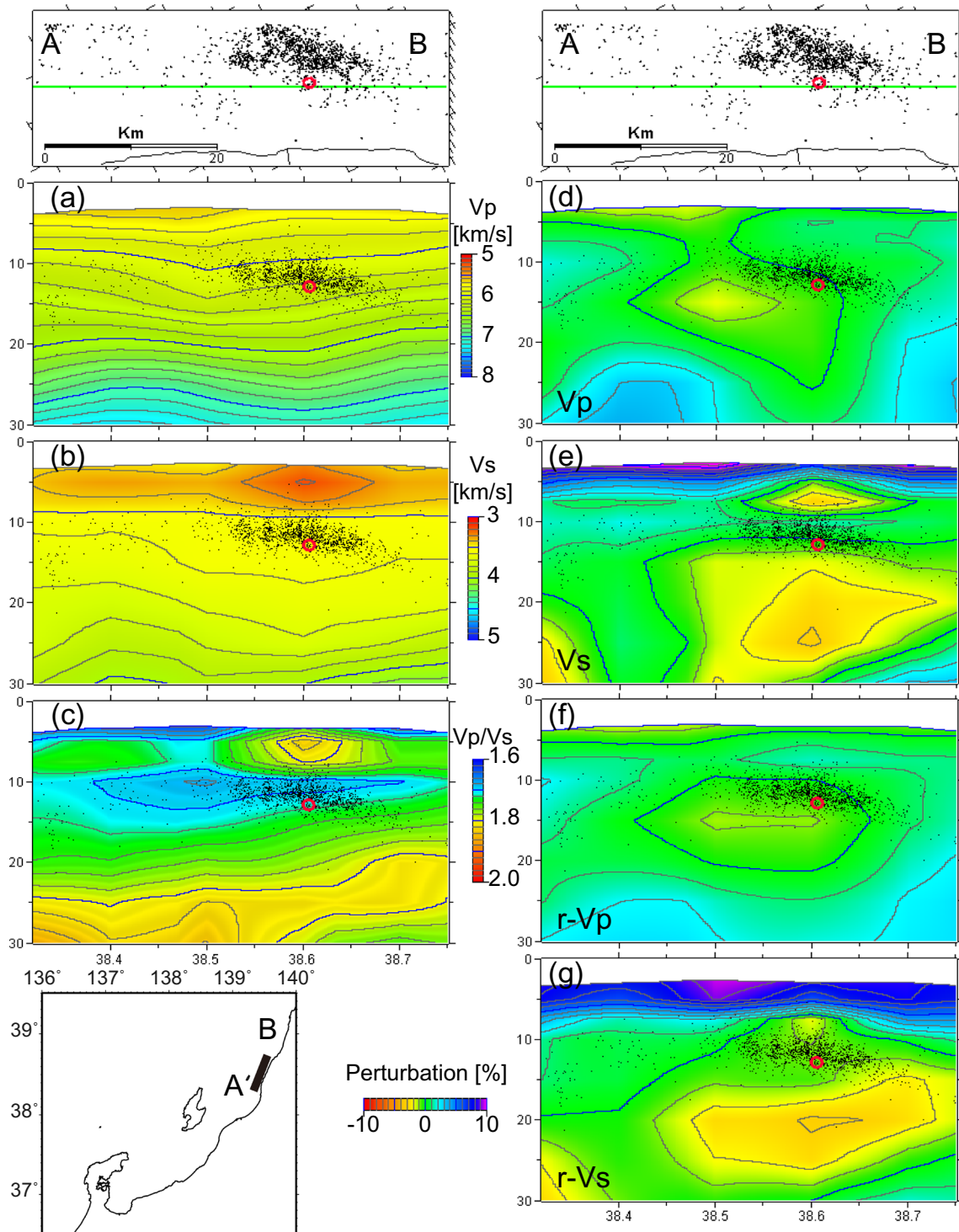
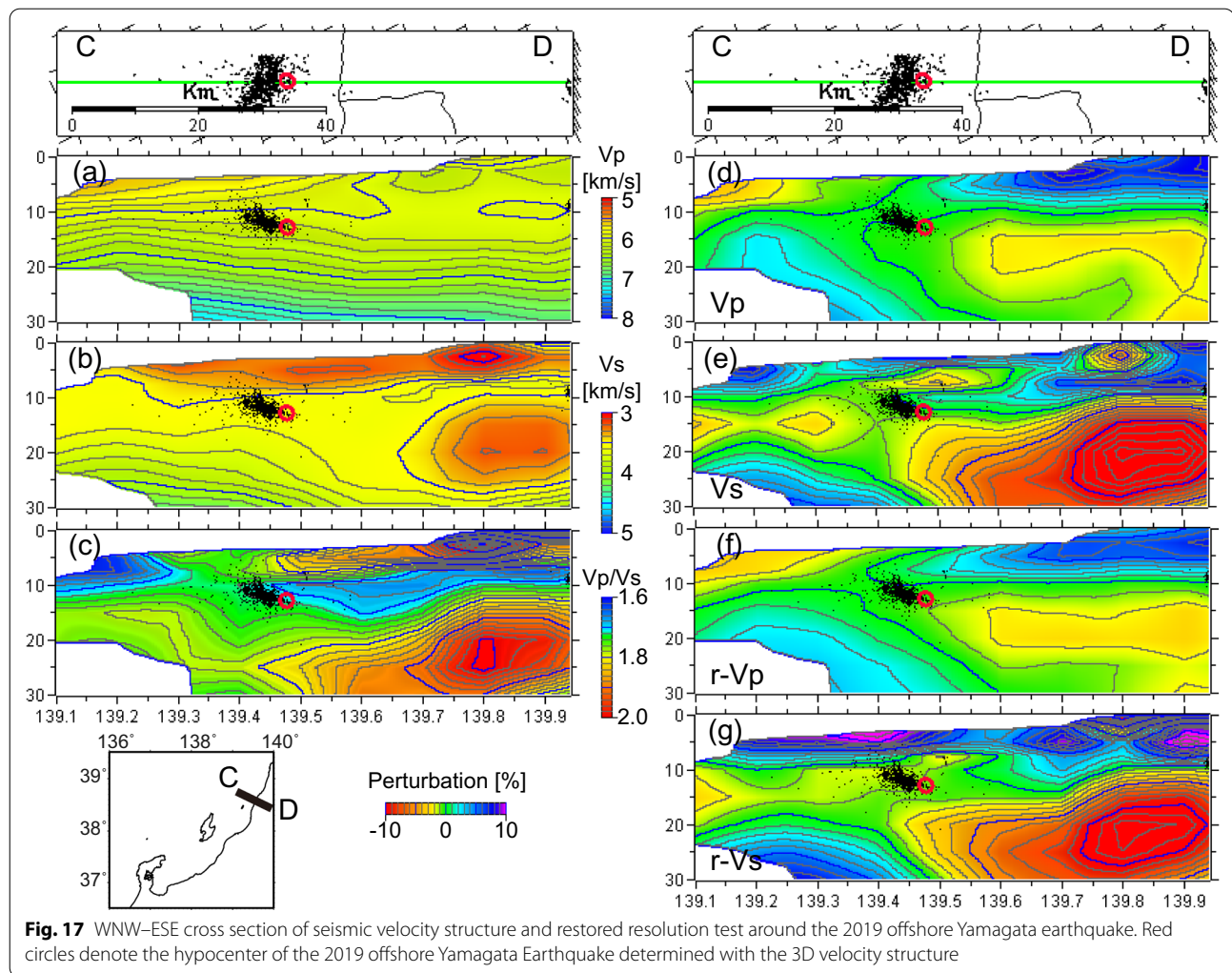


**Fig. 16** NEN-SWS cross section of seismic velocity structure and restored resolution test around the 2019 offshore Yamagata earthquake. Red circles denote the hypocenter of the 2019 offshore Yamagata Earthquake determined with the 3D velocity structure



Low-V zones are located at the MTL beneath southwestern Japan and at the northern Kinki region. A high-V zone is located between Sado Island and Noto Peninsula.

At a depth of 30 km, low-V zones are located at longitudes of 142–143° E off the eastern Japan beneath the Pacific Ocean. This low-V zone corresponds to the oceanic crust at the uppermost part of the subducting Pacific plate. The low-V zone is distributed beneath the Japanese Islands broadly at this depth. At the region along the Sea of Japan, high-V zones are imaged at the western side of the Hokkaido, around Sado Island, and around the Noto Peninsula.

At a depth of 40 km, a NNE-SSW low-V zone off the eastern Honshu coast corresponding to the low-V oceanic crust of the Pacific plate approaches Honshu. Low-V zones beneath Honshu correspond to the active volcanoes. Low-V zones from western Honshu to eastern

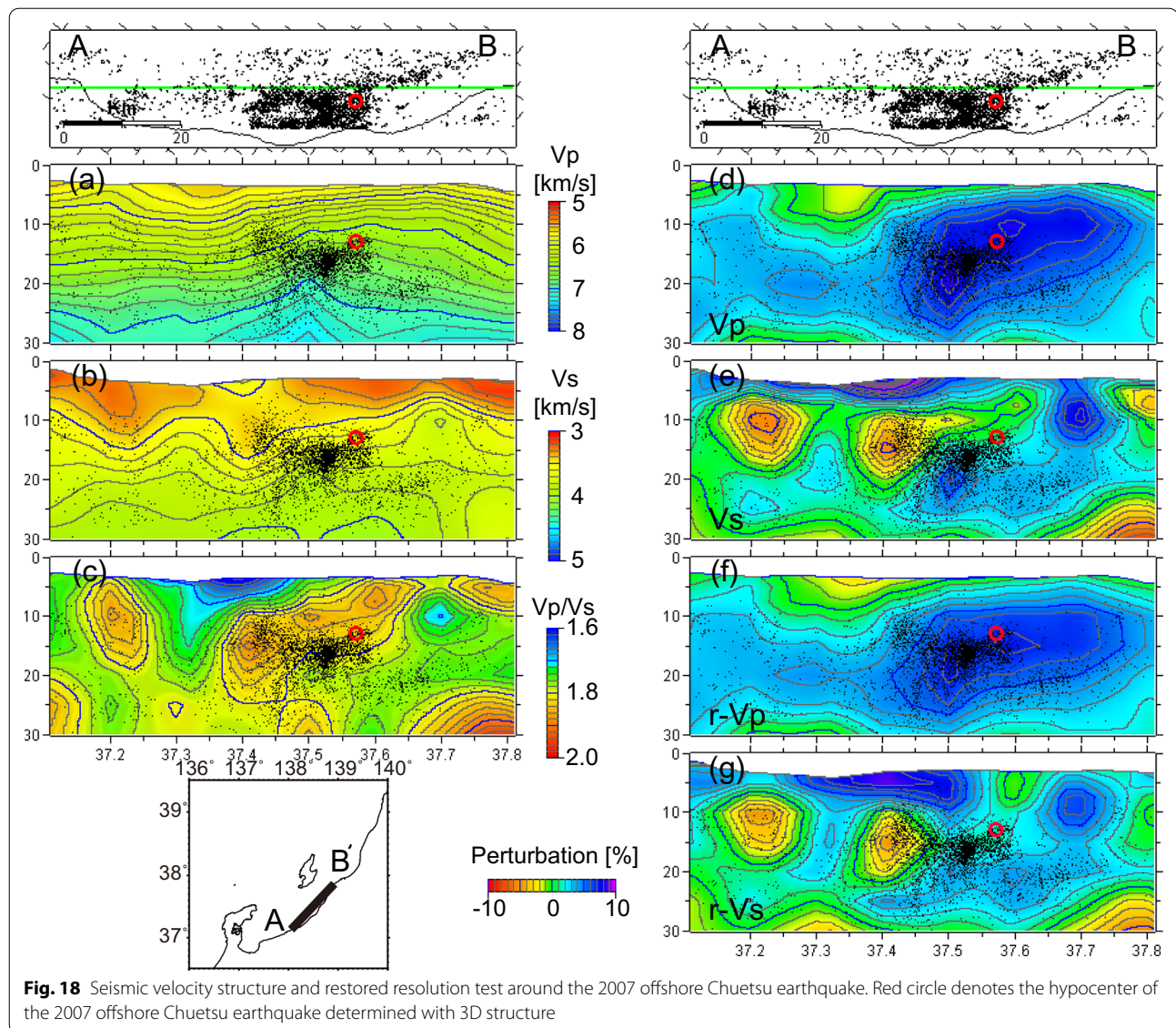
Kyushu Islands correspond to the low-V oceanic crust of the subducting Philippine Sea plate. High-V zones located on the south side of the low-V zone beneath the southwestern Japan are mantle of the subducting Philippine Sea plate.

At a depth of 60 km, high-V subducting Pacific and Philippine Sea plates and low-V oceanic crust at the uppermost parts of the Pacific plate are clearly imaged. A low-V zone exists beneath the central Honshu Island at the mountainous region and the collision zone of Honshu Island and the Izu-Bonin Arc.

#### Results of restored resolution test

We show the results of restored resolution test in Figs. 13 and 14. Comparisons between Figs. 10 and 13 and Figs. 11 and 14, show that we obtain the similar results with the final ray paths used in the inversion.





### Map views beneath the regions along the Sea of Japan

We image a quite low-V zone beneath the Sea of Japan between the Noto Peninsula and Sado Island; however, we cannot image that extremely low-V zone where we lack air gun data (Fig. 15). This shallow low-V zone is clarified first in this study because of the use of air gun data. The velocity structures including air gun data below the depth of 20 km are almost same as those without the air gun data. These results indicate that the shallow low-V zone is owing to the existence of the air gun data passing through the shallow sedimentary zone of the seafloor. This study only used the air gun data offshore Yamagata and between the Sado Island and Noto Peninsula. There are many air gun shots in the Sea of Japan by JAMSTEC and national universities. We may be able to image the

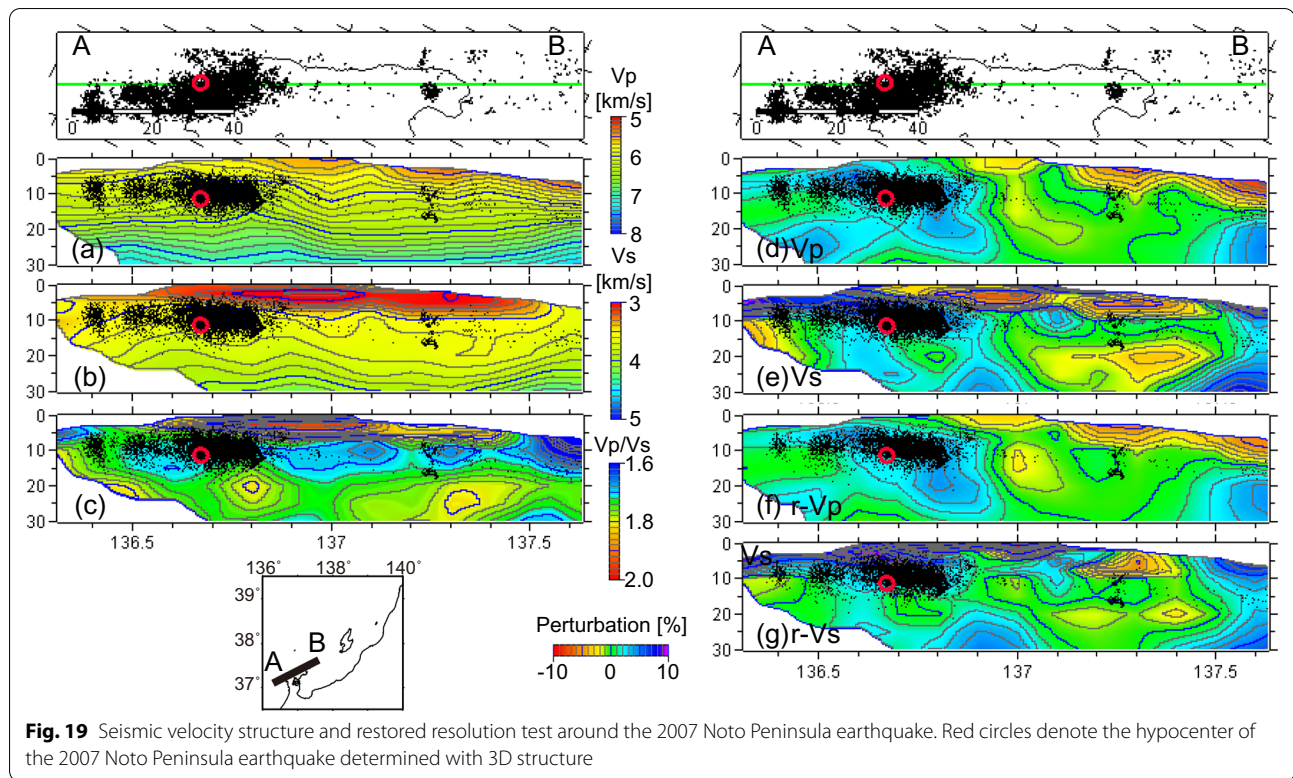
shallow low-V zone near the shore of oceans surrounding Japan if we use other offshore air gun data.

### Velocity structure beneath the large events along the Sea of Japan in the past 20 years

We relocated the all events determined by NIED Hi-net and NIED S-net from October 2000 to December 2019 with magnitudes equal to or larger than 1.5.

### The 2019 offshore Yamagata earthquake

Figures 16 and 17 show the NNE–SSW and ESE–WNW cross sections below the 2019 offshore Yamagata earthquake, respectively. The red circle denotes the mainshock with magnitude larger than 6.0. The mainshock



is located at the boundary between northwestern high- and southeastern low- $V_p$  zone (Fig. 17a, d) between the upper and lower low- $V_s$  zones (Fig. 17b, e) with low- $V_p/V_s$  zone (Fig. 17c). Aftershocks are located at the west side of the mainshock, dipping eastward (Fig. 16). Results of restored resolution tests show the similar results with those from the inversion (Figs. 16f, g, and 17f, g).

#### The 2007 offshore Chuetsu earthquake

Figure 18 shows the ENE–WSW cross sections below the 2007 offshore Chuetsu earthquake. The mainshock is located at the boundary of the upper low- $V_s$  and lower high- $V_s$  zone within the high- $V_p$  zone with 1.82  $V_p/V_s$  zone (Fig. 13a–c). The aftershocks are distributed in the high- $V_p$  zone with  $V_p/V_s$  of 1.79–1.86. Results of restored resolution tests show the similar results with those from the inversion (Fig. 18f, g) such as high- $V_p$  zone around the hypocenter and two low- $V_s$  zones on the southwest side of the hypocenter.

#### The 2007 Noto Peninsula earthquake

Figure 19 shows the ENE–WSW cross sections along the 2007 Noto Peninsula earthquake. The mainshock is located at the boundary of shallow high- $V_p$  and deeper low- $V_p$  zone and at the boundary of northern

low- $V_s$  and southern high- $V_s$  zone within the low- $V_p/V_s$  zone (Fig. 19c–e). Aftershocks are located within the high- $V_p$  and high- $V_s$  and surrounding the low- $V_p/V_s$  zone (Fig. 19c–e). Results of restored resolution tests show the similar results with those from the inversion (Fig. 19f, g) such as hypocenter at the boundary of low- $V$  and high- $V$  zones.

#### Station corrections

We calculate the station correction using the difference between the observed travel time and the calculated (theoretical) travel time (O–C). Figure 20 shows the station corrections for P- and S-wave for the final model. Red stations denote positive O–C travel times. The calculated travel time is smaller than the observed travel time. This means that the modeled velocity is too high due to the presence of thick sediment or other low- $V$  materials. The Hi-net seismometers are deployed at the bottom of boreholes typically 100–200 m deep. Some of them have depths of over 1000 m. The positive O–C stations for both P- and S-wave are located along the Sea of Japan and the Ou Backbone Range in the northeastern Japan for onshore seismic stations.

The S-net stations on the east side of the Japan Trench have negative O–C for both P- and S-wave due to the presence of high-velocity bedrock. Those between

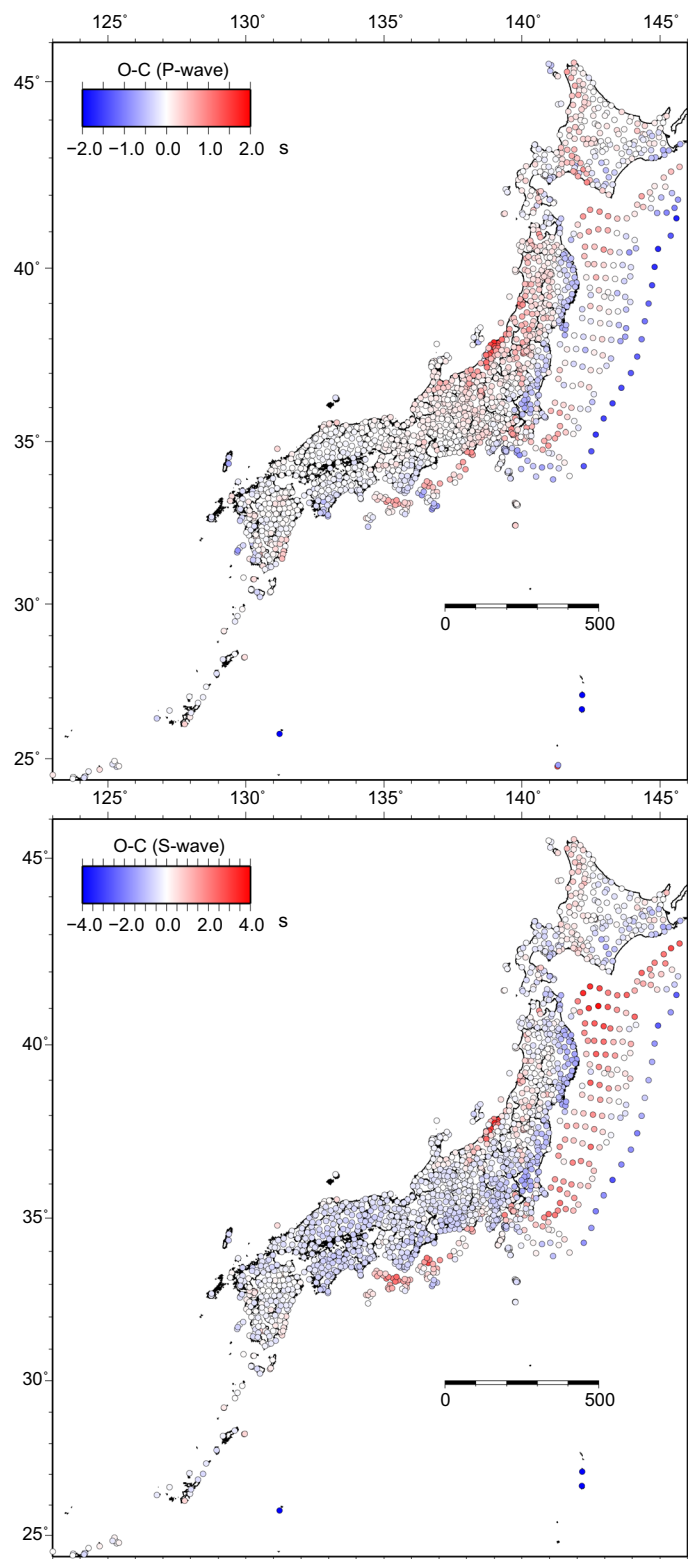


Figure 20

**Fig. 20** Station corrections for  $V_p$  and  $V_s$

Honshu and Japan Trench have positive O-C since the most of them are just laid on the seafloor with thick sediments.

The DONET stations also have positive O-C except those in the southeast offshore Kumano. Positive O-C stations are located on the sediments; however, the negative O-C stations are on the bedrock.

## Discussion

### Comparison of velocity structure beneath central Japan with previous studies

Our analysis only used the permanent seismic station data and did not include the temporary seismic stations. The Vp structures at depths of 10–25 km are almost same as those by Nakajima et al. (2010); however, unlike their results, our Vs structure does not have a low-Vs zone at depths of 15–25 km. Our Vp structure has extremely low-Vp beneath the Hida and Akaishi mountain range at depths of 40–60 km; however, Nakajima et al. (2010) did not resolve a similar feature. Our Vs structure at depths of 40–50 km beneath the Hida and Akaishi mountain range is consistent with those by Nakajima et al. (2010). They used the temporary seismic stations and their resolution size is about 10 km (half of our analysis) and they assumed the Conrad and Moho discontinuities in the inversion. We did not assume those discontinuities because the dense seismic data can image the seismic velocity structure without assuming the uncertain velocity discontinuities. The difference of structure may derive from their assumption of seismic discontinuities. Low-Vp at the uppermost mantle between the 2004 Chuetsu Earthquake and 2007 offshore Chuetsu Earthquake without the assumption of Moho discontinuity is consistent with the Vp structure by Nakajima and Hasegawa (2008) with the assumption of Moho discontinuity.

Focusing on the offshore Chuetsu earthquake region, high-Vp structure on the southeastern side of the aftershock region of the offshore Chuetsu earthquake is consistent with that by Kato et al. (2008a). A shallow low-Vp zone and a high-Vp zone on the southeastern side of the 2007 Noto Peninsula earthquake are consistent with those by Kato et al. (2008b). They used the temporary seismic stations and resolved more detailed seismic velocity structure; however, the region of good resolution is limited to the vicinity of the aftershock region.

### Coseismic slip region of the 2019 offshore Yamagata earthquake between low-V and high-V zone

Figure 21 shows the velocity structure on the coseismic slip region estimated by National Research Institute

for Earth Science and Disaster Resilience (2020). This zone is located between the southern low-Vp and the northern high-Vp and between the deeper low-Vs and the shallower high-Vs zones with 1.72–1.76 Vp/Vs. The large slip zone is at a distance of 4–10 km along dip with Vp between 6.0 and 6.5 km/s.

### The 2007 offshore Chuetsu earthquake region with high-Vp

Aftershocks determined using data from ocean bottom seismometer are located on the SE-dipping plane (Shinohara et al. 2008). The hypocenter of the 2007 offshore Chuetsu earthquake is located at the bottom of the extremely high-Vp and high-Vp/Vs zone (Yukutake et al. 2008). Large coseismic slip region is shallow zone (Aoi et al. 2008) with Vp of 6.0–6.3 km/s and Vp/Vs of 1.72–1.76 (Fig. 22). JAMSTEC conducted the reflection survey (No et al. 2009) and Nakahigashi et al. (2012) estimated the seismic velocity structure with refraction seismology. Their result shows a low-Vp zone less than 3.0 km/s at depths shallower than 3 km and high-Vp between 7.0 and 7.2 km/s at depths of 13–24 km. Our result shows 5.5 km/s Vp zone at depths below 10 km depth and 6 km/s Vp zone at depths of 12–13 km and 6.5 km/s Vp at depths around 15 km beneath the Sea of Japan, and 7.0–7.2 km/s Vp at depths of 20–25 km (Fig. 23). Seismic tomography is not good at estimating a precise velocity boundary; however, low-Vp upper crust and high-V lower crust beneath the Sea of Japan and high-V upper crust and low-V lower crust beneath the Honshu is consistent with their result (Fig. 23).

### The 2007 Noto Peninsula earthquake region with high-Vp and Vs

The hypocenter of the 2007 Noto Peninsula earthquake is located within a high-Vp and high-Vs region (Hiramatsu et al. 2008). The coseismic slip region by Pulido et al. (2008) is also located within a high-Vp and high-Vs zone surrounding hypocenter. The largest slip region is the shallowmost zone; however, the seismic tomography clarified the seismic velocity structure below a depth of 3–5 km for Vp since there is neither reflection nor refraction seismic data on the west side of the Noto peninsula.

Starting in July 2021, microseismicity became active at the northeastern tip of the Noto Peninsula. This zone has a high-Vp and slightly high-Vp/Vs (1.74–1.78) zone between the low-Vp and low-Vp/Vs (1.65–1.70) zones (Fig. 19).

### High-V zone beneath the Mogami Trough and Sado Ridge

The region from the Sado Ridge to Mogami Trough was formed by uplift of a half-graben owing to the inversion tectonics (Okamura 2000). We used the air



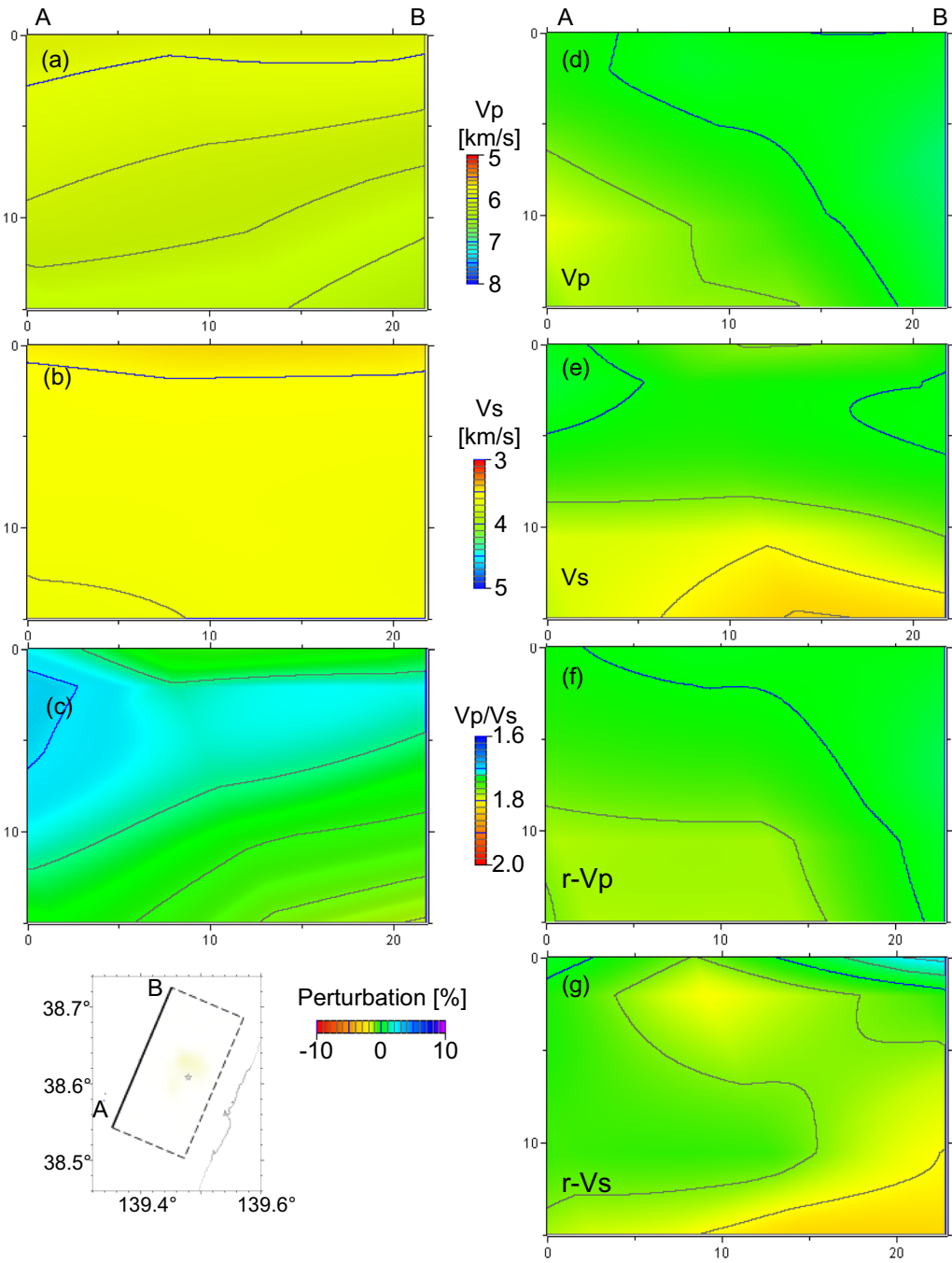


**Fig. 21** Seismic velocity structure and restored resolution test along the coseismic slip region of the 2019 offshore Yamagata earthquake



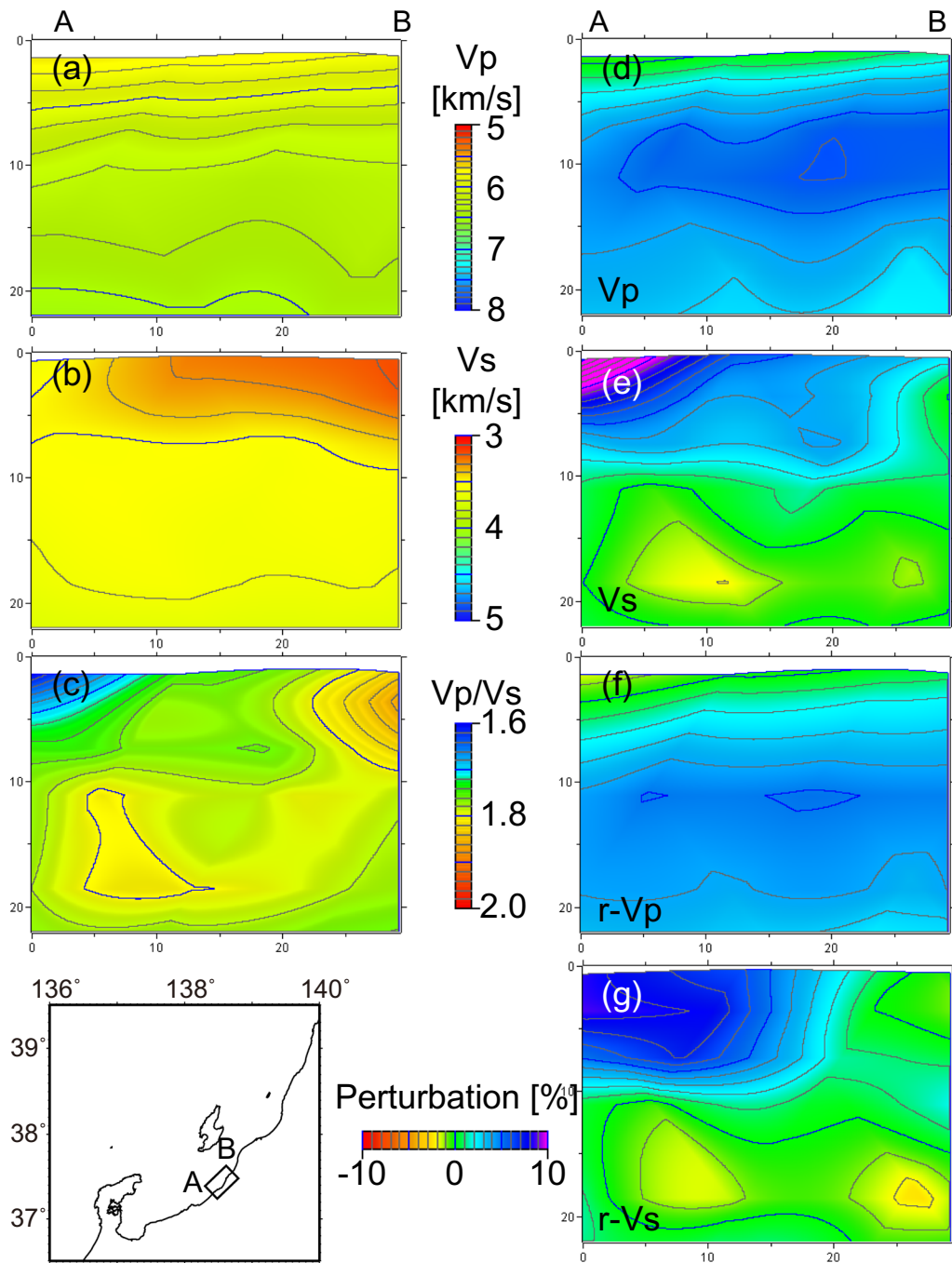
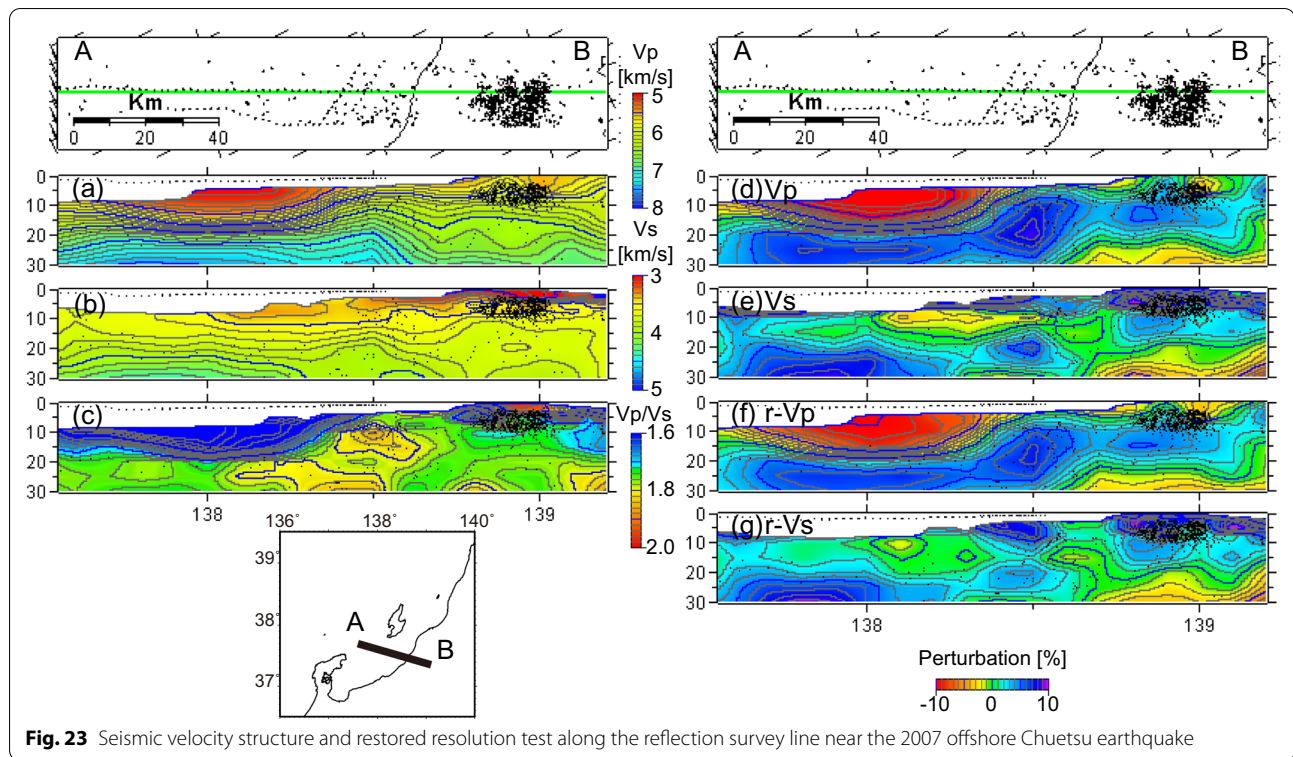


**Fig. 22** Seismic velocity structure and restored resolution test along the coseismic slip region of the 2007 offshore Chuetsu earthquake



gun data along Mogami Trough. The west side of the hypocenter of the 2019 offshore Yamagata earthquake at depths of 10–30 km has high-V corresponding to the Mogami Trough (Fig. 24). This high-V lower crust passes through Awa Island and reaches Sado Basin between Sado Island and Honshu. A major rift zone in the Tohoku Arc runs from the Akita to Niigata region along the coast of Sea of Japan (Sato 1994) and corresponds to high-V lower crust and a shallow Moho corresponds to the failed rift zone (Matsubara et al. 2017a, 2019).

### Conclusion

We conducted the seismic tomography for entire Japanese Islands including the Sea of Japan and the Pacific Ocean using arrival times from reflection seismology. We can image the shallow zone along the Sea of Japan from offshore Yamagata to Noto Peninsula by using the

air gun data. The extremely low-V shallow zone is imaged between Sado Island and Noto Peninsula. We also obtain detailed seismic velocity structure beneath the Pacific Ocean at depths of 20–50 km owing to the S-net data.

The 2007 Noto Peninsula, the 2007 offshore Chuetsu-, and the 2019 offshore Yamagata earthquakes occurred at the boundary between high-Vp and low-Vp zones. Low-Vp upper crust and high-V lower crust beneath the Sea of Japan and high-V upper crust and low-V lower crust beneath Honshu are imaged by reflection seismology near the offshore Chuetsu earthquake.

The west side of the hypocenter of the 2019 offshore Yamagata earthquake at depths of 10–30 km has high-V corresponding to the Mogami Trough. This high-V zone passes through Awa Island and reaches Sado Basin between Sado Island and Honshu. A major rift zone in the Tohoku Arc from Akita to Niigata region along the coast of Sea of Japan corresponds to high-V lower crust and a shallow Moho.

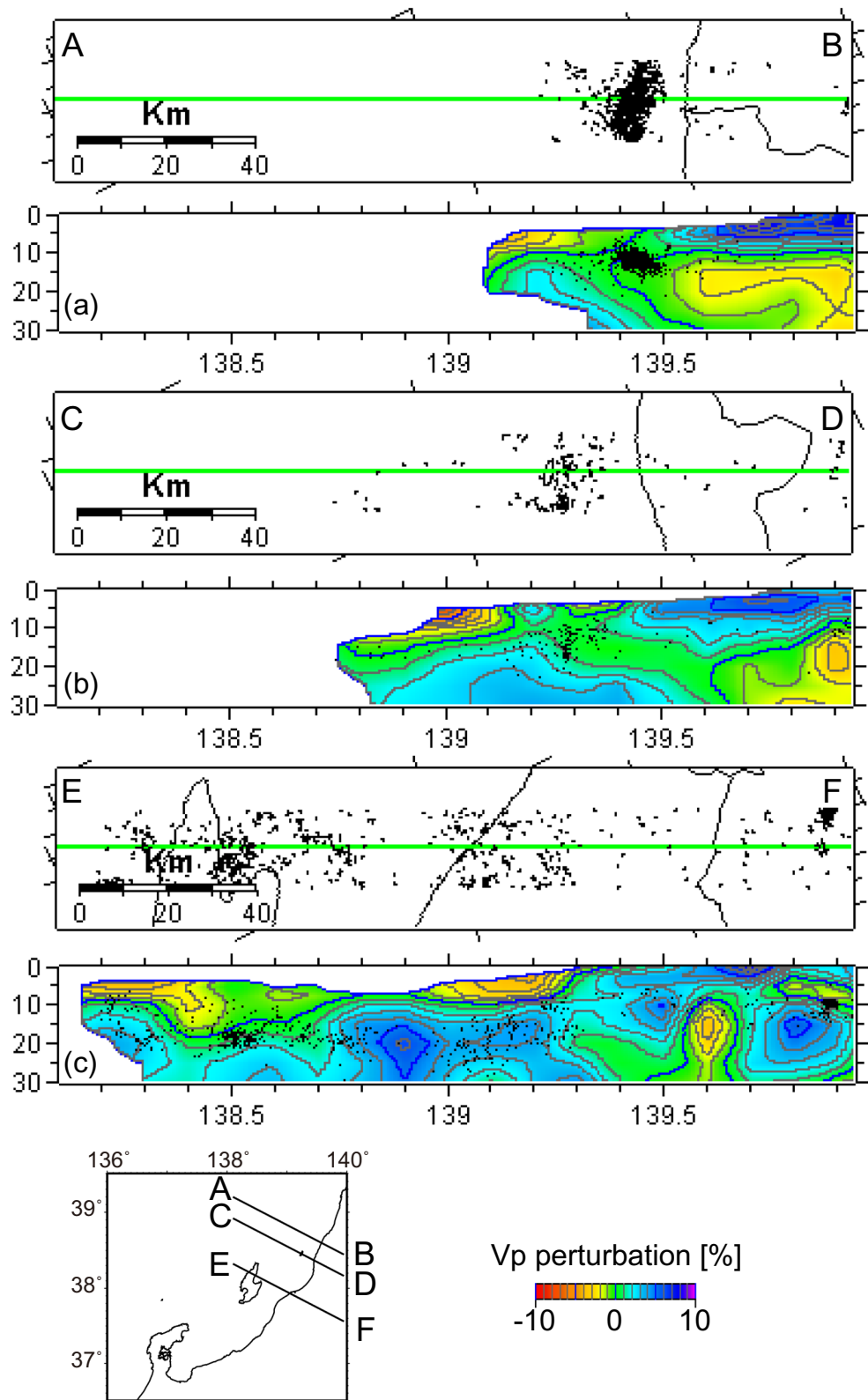


**Fig. 24** Vertical cross section across Mogami Trough and rift along the coast of Sea of Japan. **a** Across the hypocenter of 2019 offshore Yamagata earthquake, **b** across the Awa Island, and **c** across the Sado Basin

## Acknowledgements

We used the seismic data provided by the National Research Institute for Earth Science and Disaster Resilience, the Japan Meteorological Agency, Hokkaido University, Hirosaki University, Tohoku University, the University of Tokyo, Nagoya University, Kyoto University, Kochi University, Kyushu University, Kagoshima University, the National Institute of Advanced Industrial Science and Technology, the Geographical Survey Institute, Tokyo Metropolis, Shizuoka Prefecture, Hot Springs Research Institute of Kanagawa Prefecture, Yokohama City, and Japan Agency for Marine-Earth Science and Technology. This study was supported by the Advanced Earthquake and Tsunami Forecasting Technologies Project for NIED. Some of the figures were drawn using Generic Mapping Tools software (Wessel and Smith 1995) and the software for viewing 3D velocity structures beneath the entire Japan islands (Matsubara 2010). This work was financially supported in part by the project on the Investigation of Earthquake and Tsunami along the Sea of Japan by Japanese Ministry of Education, Culture, Sports, Science, and Technology (MEXT). We thank David Shelly for editing our draft. We are grateful to two anonymous reviewers for instructive comments.

## Author contributions

MM analyzed the seismic tomogram and summarized this paper. TI gave the geological and tectonic advice. TN gave the information of air gun shot data. KU, MM, TK supplied the NIED S-net data, NT and SK supplied the NIED DONET data. All authors read and approved the final manuscript.

## Funding

This study was supported by the Advanced Earthquake and Tsunami Forecasting Technologies Project for NIED (National Research Institute for Earth Science and Disaster Resilience). This work was financially supported in part by the project on the Investigation of Earthquake and Tsunami along the Sea of Japan by Japanese Ministry of Education, Culture, Sports, Science, and Technology (MEXT).

## Availability of data and materials

All waveforms of NIED Hi-net and S-net are available from the NIED web site.

## Declarations

## Competing interests

The authors declare that they have no competing interests.

## Author details

<sup>1</sup>National Research Institute for Earth Science and Disaster Resilience, 3-1 Tennodai, Tsukuba, Ibaraki 305-0006, Japan. <sup>2</sup>Earthquake Research Institute, The University of Tokyo, 1-1-1 Yayoi, Bunkyo, Tokyo 113-0032, Japan. <sup>3</sup>Japan Agency for Marine-Earth Science and Technology, 3173-25 Showamachi, Kanazawa, Yokohama, Kanagawa 236-0001, Japan. <sup>4</sup>Association for the Development of Earthquake Prediction, 1-5-18 Kandasarugaku-Cho, Chiyoda, Tokyo 101-0064, Japan.

Received: 6 January 2022 Accepted: 18 October 2022

Published online: 22 November 2022

## References

- Aoi S, Sekiguchi H, Morikawa N, Kunugi T (2008) Source process of the 2007 Niigata-ken Chuetsu-oki earthquake derived from near-fault strong motion data. *Earth Planets Space* 60:1131–1135. <https://doi.org/10.1186/BF03353149>
- Asano Y, Saito T, Ito Y, Shiomi K, Hirose H, Matsumoto T, Aoi S, Hori S, Sekiguchi S (2011) Spatial distribution and focal mechanisms of aftershocks of the 2011 off the Pacific coast of Tohoku Earthquake. *Earth Planets Space* 63:669–673. <https://doi.org/10.5047/eps.2011.06.016>
- Hiramatsu Y, Moriya K, Kamiya T, Kato M, Nishimura T (2008) Fault model of the 2007 Noto Hanto earthquake estimated from coseismic deformation obtained by the distribution of littoral organisms and GPS: implication for neotectonics in the northwestern Noto Peninsula. *Earth Planets Space* 60:903–913. <https://doi.org/10.1186/BF03352846>
- Kanazawa T (2013) Japan Trench earthquake and tsunami monitoring network of cable-linked 150 ocean bottom observatories and its impact to earth disaster science. In: 2013 IEEE international underwater technology symposium (UT), IEEE, pp 1–5
- Kato A, Sakai S, Iidaka T, Iwasaki T, Kurashimo E, Igarashi T, Hirata N, Kanazawa T, Group for the aftershock observations of the 2007 Noto Hanto Earthquake (2008a) Three-dimensional velocity structure in the source region of the Noto Hanto Earthquake in 2007 imaged by a dense seismic observation. *Earth Planets Space* 60:105–110. <https://doi.org/10.1186/BF03352769>
- Kato A, Sakai S, Kurashimo E, Igarashi T, Iidaka T, Hirata N, Iwasaki T, Kanazawa T, Group for the aftershock observations of the 2007 Niigataken Chuetsu-oki Earthquake (2008b) Imaging heterogeneous velocity structures and complex aftershock distributions in the source region of the 2007 Niigataken Chuetsu-oki Earthquake by a dense seismic observation. *Earth Planets Space* 60:1111–1116. <https://doi.org/10.1186/BF03353145>
- Koketsu K, Sekine S (1998) Pseudo-bending method for three-dimensional seismic ray tracing, in a spherical Earth with discontinuities. *Geophys J Int* 132:427–434. <https://doi.org/10.1046/j.1365-246x.1998.00427.x>
- Matsubara M (2010) Software for viewing 3D velocity structures beneath whole Japan Islands, Report of the National Research Institute for Earth Science and Disaster Resilience. 76:1–9. <https://doi.org/10.24732/nied.00001198>
- Matsubara M, Obara K (2011) The 2011 Off the Pacific Coast of Tohoku earthquake related to a strong velocity gradient with the Pacific plate. *Earth Planets Space* 63:663–667. <https://doi.org/10.5047/eps.2011.05.018>
- Matsubara M, Hirata N, Sato H, Sakai S (2004) Lower crustal fluid distribution in the northeastern Japan arc revealed by high resolution 3D seismic tomography. *Tectonophysics* 388:33–45. <https://doi.org/10.1016/j.tecto.2004.07.046>
- Matsubara M, Hayashi H, Obara K, Kasahara K (2005) Low-velocity oceanic crust at the top of the Philippine Sea and Pacific plates beneath the Kanto region, central Japan, imaged by seismic tomography. *J Geophys Res* 110:B12304. <https://doi.org/10.1029/2005JB003673>
- Matsubara M, Obara K, Kasahara K (2008) Three-dimensional P- and S-wave velocity structures beneath the Japan Islands obtained by high-density seismic stations by seismic tomography. *Tectonophysics* 454:86–103. <https://doi.org/10.1016/j.tecto.2008.04.016>
- Matsubara M, Sato H, Ishiyama TV, Horne AD (2017a) Configuration of the Moho discontinuity beneath the Japanese Islands derived from three-dimensional seismic tomography. *Tectonophysics* 710–711:97–107. <https://doi.org/10.1016/j.tecto.2016.11.025>
- Matsubara M, Sato H, Uehira K, Mochizuki M, Kanazawa T (2017b) Three-dimensional seismic velocity structure beneath Japanese Islands and surroundings based on NIED seismic networks using both inland and offshore events. *J Disaster Res* 12:844–857. <https://doi.org/10.20965/jdr.2017.p0844>
- Matsubara M, Sato H, Uehira K, Mochizuki M, Kanazawa T, Takahashi N, Suzuki K, Kamiya S, Matsubara M, Sato H, Uehira K, Mochizuki M, Kanazawa T, Takahashi N, Suzuki K, Kamiya S (2019) Seismic velocity structure in and around the Japanese Island arc derived from seismic tomography including NIED MOWLAS Hi-net and S-net data, seismic waves—probing earth system. *IntechOpen*, London, pp 1–19. <https://doi.org/10.5772/intechopen.86936>
- Nakahigashi K, Shinohara M, Kurashimo E, Yamada T, Kato A, Takanami T, Uehira K, Ito Y, Iidaka T, Igarashi T, Sato H, Hino R, Obara K, Kaneda Y, Hirata N, Iwasaki T, Kanazawa T (2012) Seismic structure of the source region of the 2007 Chuetsu-oki earthquake revealed by offshore-onshore seismic survey: asperity zone of intraplate earthquake delimited by crustal inhomogeneity. *Tectonophysics* 562–563(2012):34–47. <https://doi.org/10.1016/j.tecto.2012.06.052>
- Nakajima J, Hasegawa A (2008) Existence of low-velocity zones under the source areas of the 2004 Chuetsu and 2007 Chuetsu-oki earthquakes inferred from travel-time tomography. *Earth Planets Space* 60:1127–1130. <https://doi.org/10.1186/BF03353148>
- Nakajima J, Kato A, Iwasaki T, Ohmi S, Okada T, Takeda T (2010) Deep crustal structure around the Atotsugawa fault system, central Japan: a weak zone below the seismogenic zone and its role in earthquake generation. *Earth Planets Space* 62:555–566. <https://doi.org/10.5047/eps.2010.06.007>



- National Research Institute for Earth Science and Disaster Resilience (2019a) NIED Hi-net, National Research Institute for Earth Science and Disaster Resilience. <https://doi.org/10.17598/NIED.0003>
- National Research Institute for Earth Science and Disaster Resilience (2019b) NIED DONET, National Research Institute for Earth Science and Disaster Resilience. <https://doi.org/10.17598/NIED.0008>
- National Research Institute for Earth Science and Disaster Resilience (2019c) NIED MOWLAS, National Research Institute for Earth Science and Disaster Resilience. <https://doi.org/10.17598/NIED.0009>
- National Research Institute for Earth Science and Disaster Resilience (2019d) NIED S-net, National Research Institute for Earth Science and Disaster Resilience. <https://doi.org/10.17598/NIED.0004>
- National Research Institute for Earth Science and Disaster Resilience (2020) Rupture process of the 2019 off Yamagata prefecture earthquake derived from near-source strong-motion records, report of Coordinating Committee for Earthquake Prediction, Japan. 103:73–77. [https://cais.gsi.go.jp/YOCHIREN/report/kaihou103/03\\_05.pdf](https://cais.gsi.go.jp/YOCHIREN/report/kaihou103/03_05.pdf)
- No T, Takahashi N, Kodaira S, Obana K, Kaneda Y (2009) Characteristics of deformation structure around the 2007 Niigata-ken Chuetsu-oki earthquake detected by multi-channel seismic reflection imaging. *Earth Planets Space* 61:1111–1115. <https://doi.org/10.1186/BF03352961>
- No T, Sato T, Kodaira S, Takahashi N, Ishiyama T, Sato T, Kaneda Y (2014) Multichannel seismic reflection survey in the eastern part of the Japan Sea, JAMSTEC Rep. Res Dev 19:29–47. <https://doi.org/10.5918/jamstec.19.29>
- Nolet G (1987) Seismic tomography. D. Reidel Publishing Company, Dordrecht
- Obara K, Kasahara K, Hori S, Okada Y (2005) A densely distributed high-sensitivity seismograph network in Japan: Hi-net by National Research Institute for Earth Science and Disaster Prevention. *Rev Sci Instrum* 76:021301. <https://doi.org/10.1063/1.1854197>
- Okada Y, Kasahara K, Hori S, Obara K, Sekiguchi S, Fujiwara H, Yamamoto A (2004) Recent progress of seismic observation networks in Japan—Hi-net F-net, K-NET and KiK-net. *Earth Planets Space* 56:xv–xxviii. <https://doi.org/10.1186/BF03353076>
- Okamura Y (2000) Inversion tectonics along the eastern margin of the Japan Sea. *J Jap Assoc Petroleum Tech* 65:40–47 (**in Japanese with English abstract**)
- Pulido N, Aoi S, Fujiwara H (2008) Rupture process of the 2007 Notohanto earthquake by using an isochrones back-projection method and K-NET/KiK-net data. *Earth Planets Space* 60:1035–1040. <https://doi.org/10.1186/BF03352865>
- Sato H (1994) The relationship between late Cenozoic events and stress field and basin development in northeast Japan. *J Geophys Res* 99:22261–22274. <https://doi.org/10.1029/94JB00854>
- Shinohara M, Kanazawa T, Yamada T, Nakahigashi K, Sakai S, Hino R, Murai Y, Yamazaki A, Obana K, Ito Y, Iwakiri K, Miura R, Machida Y, Mochizuki K, Uehira K, Tahara M, Kuwano A, Amamiya S, Kodaira S, Takanami T, Kaneda Y, Iwasaki T (2008) Precise aftershock distribution of the 2007 Chuetsu-oki earthquake obtained by using an ocean bottom seismometer network. *Earth Planets Space* 60:1121–1126. <https://doi.org/10.1186/BF03353147>
- Uehira K, Kanazawa T, Mochizuki M, Fujimoto H, Noguchi S, Shinbo T, Shiomi K, Kunugi T, Aoi S, Matsumoto T, Sekiguchi S, Okada Y, Shinohara M, Yamada T (2016) Outline of seafloor observation network for earthquakes and tsunamis along the Japan Trench (S-net), EGU General Assembly 2016, EGU2016-13832
- Ukawa M, Ishida M, Matsumura S, Kasahara K (1984) Hypocenter determination method of the Kanto-Tokai observational network for microearthquakes. *Res Notes Natl Res Cent Disaster Prev* 53:1–88 (**in Japanese with English abstract**)
- Wessel P, Smith WHF (1995) New version of generic mapping tools released. *EOS Trans AGU* 79:329
- Yukutake Y, Takeda T, Obara K (2008) Well-resolved hypocenter distribution using the double-difference relocation method in the region of the 2007 Chuetsu-oki Earthquake. *Earth Planets Space* 60:1105–1109. <https://doi.org/10.1186/BF03353144>
- Zhao D, Hasegawa A, Horiuchi S (1992) Tomographic imaging of P and S wave velocity structure beneath northeastern Japan. *J Geophys Res* 97:19909–19928
- Zhao D, Huang Z, Umino N, Hasegawa A, Kanamori H (2011) Structural heterogeneity in the megathrust zone and mechanism of the 2011 Tohoku-Oki earthquake (Mw 9.0). *Geophys Res Lett* 38(17):17308. <https://doi.org/10.1029/2011GL048408>
- Zhao D, Kitagawa H, Toyokuni G (2015) A water wall in the Tohoku forearc causing large crustal earthquakes. *Geophys J Int* 200:149–172. <https://doi.org/10.1093/gji/ggu381>

## Publisher's Note

Springer Nature remains neutral with regard to jurisdictional claims in published maps and institutional affiliations.

**Submit your manuscript to a SpringerOpen<sup>®</sup> journal and benefit from:**

- Convenient online submission
- Rigorous peer review
- Open access: articles freely available online
- High visibility within the field
- Retaining the copyright to your article

Submit your next manuscript at ► [springeropen.com](https://www.springeropen.com)